

Architectural structures from quad meshes with planar parameter lines

Cheng Wang^a, Caigui Jiang^{a,b}, Hui Wang^a, Xavier Tellier^c, Helmut Pottmann^{a,*}

^aKing Abdullah University of Science and Technology, P.O. Box 2187, 4700 Thuwal, 23955-6900, Kingdom of Saudi Arabia

^bXi'an Jiaotong University, No.28 Xianning West Road, Xi'an, 710049, China

^cNavier Laboratory (Ecole des Ponts, UGE, CNRS), 6 av. Blaise Pascal, 77420, Champs-sur-Marne, France

Abstract

We address the computational design of architectural structures which are based on a frame of intersecting beams that are aligned with the parameter lines of a quad mesh. While previous work mainly put a planarity constraint onto the faces of the mesh, we focus on the planarity of long-range supporting beams which follow selected polylines in the underlying mesh. In addition to that, we impose further constraints including planarity of faces, right node angles and static equilibrium, and discuss in which way these may be combined. Some of the studied meshes are discrete counterparts of certain well-known surfaces in classical geometry, whose knowledge is helpful for initializing the proposed optimization algorithms.

Keywords: architectural geometry, computational design, computational fabrication, planar parameter lines, quad mesh, planar quad mesh, support structure, gridshell, funicularity, static equilibrium

1. Introduction

The design and fabrication of freeform shapes in contemporary architecture is a rich source for challenging problems in geometric computing [1]. An important type of structure possesses a quad mesh with regular combinatorics and possibly isolated combinatorial singularities as a basic underlying geometric model. The edges of the mesh are aligned with supporting beams and the faces correspond to panels. The cost of manufacturing panels and beams is an important factor in the fabrication of such a structure. A lot of attention has so far been payed to simple panels, in particular to flat ones. Much less do we know about the design of structures from planar long-range supporting beams which follow the dominant mesh polylines (parameter lines) in the quad mesh. Geometrically, this amounts to the design of quad meshes where one or both families of parameter lines are planar. Such structures are discrete versions of smooth surfaces with one or two families of planar iso-parameter lines. Planarity of long-range elements has a global influence on the overall shape, which becomes especially tricky if one pairs this with additional constraints such as planarity of faces, static equilibrium or right node angles. The present paper contributes to exactly these requirements, but does not study structures with two families of planar polylines and planar panels, since those have recently been carefully studied [2].

1.1. Planar beams in architectural structures

1.1.1. Beam continuity

There are three possible ways to connect beams in a grid structure:

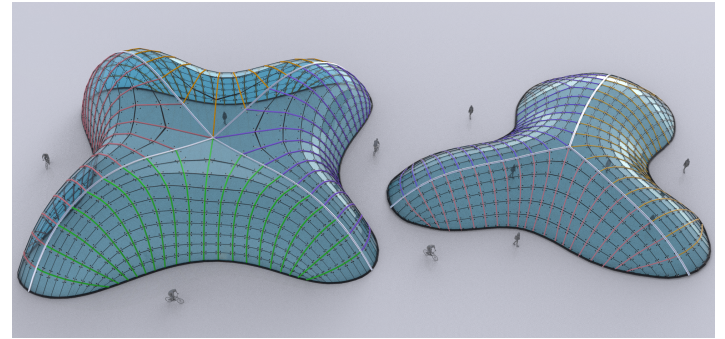


Figure 1: Left: A quad mesh with planar faces and one family of piecewise planar polylines (in colors) approximating the surface on the top of the Lilium Tower model by Zaha Hadid Architects. The detail of this design is discussed in Subsection 2.2 and Fig. 8. Right: A quad mesh in static equilibrium rationalized with planar faces and one family of piecewise planar polylines (in colors). The detail of this design is discussed in Subsection 3.2 and Fig. 13.

- 30 • Beams are continuous throughout nodes, such as in the Schubert club band shell [3] (Fig. 2 (a)), where one family of beams is stacked on top of the other.
- 31 • Beams are interrupted at nodes, such as in the gridshell of the Joe and Rika Mansueto library [4] (Fig. 2 (b)), where the straight beams are connected at nodes with curvature concentration.
- 32 • In hybrid cases, beams are continuous in only one direction, and discontinuous in the others. This is for example the case for the timber structures of the Cité du Vin in Bordeaux (Fig. 2 (c)) and the Seville Parasol [5], and for the steel structure of the Sage Gateshead music center [6].

In gridshells, beam continuity shows advantages in simplifying connections and making them stiffer. It is also studied that a timber gridshell with continuous beams can significantly reduce the environmental footprint [7]. This paper will focus on structures with continuous beams, including cases

*Corresponding author

Email addresses: cheng.wang@kaust.edu.sa (Cheng Wang), caigui.j@gmail.com (Caigui Jiang), hui.wang.10@kaust.edu.sa (Hui Wang), xavier.tellier@enpc.fr (Xavier Tellier), helmut.pottmann@kaust.edu.sa (Helmut Pottmann)



Figure 2: Planar beams in architectural structures. (a) Schubert Club Band Shell, designed by James Carpenter Design Associates (image from [flickr.com](#) photographed by Tony Webster under CC BY-SA 2.0). (b) Joe and Rika Mansueto Library, designed by Murphy/Jahn in 2011 (image from [wikimedia.org](#) photographed by Michael Barera under CC BY-SA 4.0). (c) La Cité du Vin in Bordeaux, designed by Anouk Legendre and Nicholas Desmazières of XTU Agency in 2016 (image from [flickr.com](#) photographed by Adrien Sifre under CC BY-NC-ND 2.0).

48 1 and 3. In these cases, planarity of the continuous beams
49 yields remarkable advantages in both beam fabrication and
50 structural performance.

51 1.1.2. Advantages of planar beams

52 *Fabrication.* Beams are usually fabricated from timber or
53 steel. A common method to fabricate timber beams is glu-
54 ing laminated timber. Such beams are produced by glu-
55 ing wooden strips which are bent in a plane. If a beam is not
56 planar, each strip needs to be further subdivided into rods
57 (Fig. 3 (a) and (b)) so that manufacturing complexity in-
58 creases drastically. Steel beams are commonly produced by
59 a roller bender from initially straight beams (Fig. 3 (d)). In
60 this process, it is difficult to obtain non-planar beams with
61 sufficient precision since the three rollers should be aligned
62 in a plane. Therefore for both timber and steel, the fabri-
63 cation of long-range planar beams is much cheaper and more
64 effective.

65 *Structural performance.* The planarity of beams also of-
66 fers structural benefits. A straightforward advantage is that
67 beam planarity in both directions yields a torsion-free sup-
68 port structure which can simplify the node manufacturing [8].
69 It can also facilitate the construction of multi-layer gridshells,
70 such as in the Chinese National Center of Performing Arts.
71 In addition, planar continuous beams provide convenience for
72 the installation of structural diaphragms. Cable diaphragms
73 are for example used in the Strasbourg train station to make
74 beams slender and thus obtain a remarkably light structure
75 [9] (Fig. 3 (c)). Another example is the cable reinforce-
76 ment on the glass roof of Hamburg history museum [10]. The de-
77 sign of such diaphragms based on conics was recently studied
78 in [11].

79 1.2. Compatibility of planar parameter lines with further con- 80 straints

81 Planar parameter lines can be easily achieved by intersect-
82 ing a surface with one family or two families of planes. How-
83 ever, they are no longer easy tasks when combining planar
84 parameter lines with further constraints, such as planarity of
85 faces, static equilibrium or right node angles. Hence, this pa-
86 per focuses on investigating how planar parameter lines can
87 be combined with other commonly seen constraints in archi-
88 tectural construction. Another motivation of this paper is to

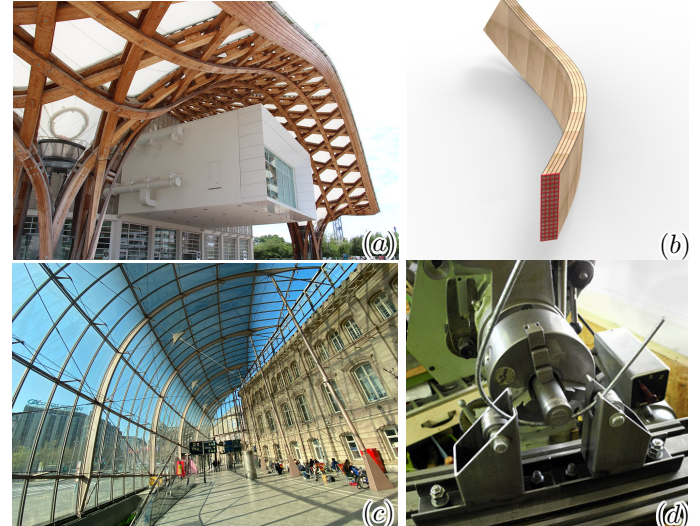


Figure 3: (a) Non-planar timber beams, such as the ones of the Centre Pompidou Metz (designed by Shigeru Ban), are curved in two directions (image from [flickr.com](#) photographed by Fred Romero under CC BY 2.0). (b) Hence, when fabricated by gluing laminated timber, the wooden strips must be subdivided into an array of rods (highlighted in red). (c) In the gridshell structure of the Strasbourg train station (designed by AREP), the planar beams are made from steel and can easily be reinforced by “bike-wheel” cable diaphragms. (d) A roller bender bends the steel with three rollers in a plane (image from [flickr.com](#) photographed by Fred Romero under CC BY-ND 2.0).

89 identify those constraint sets which allow one to represent ar-
90 bitrary freeform shapes, and separate them from those which
91 yield a restricted class of surfaces. The latter case is more
92 frequent, but in view of applications in architecture, it is not
93 an obstacle.

94 In fact, the constraints studied in this paper come from
95 practical considerations in connection with the architectural
96 application. We summarize these constraints and designate
97 their respective abbreviations in Table 1.

98 A desirable feature in architectural design is planar quad
99 panels. These are easily achieved with translational shells, as
100 seen at the Joe and Rika Mansueto library [4] (Fig. 2 (b)),
101 and the Hippo House in the Berlin zoo [6]. Moreover, all
102 quad meshes with planar faces and planar parameter lines

Abbreviations	Constraints	Figures
P	planar beams in one family	
PP	planar beams in both families	
PQ	planar quad faces	
F	funicularity (static equilibrium) with a vertical load	
90°	orthogonal crossing beams (right node angle)	

Table 1: Overview of constraints studied in this paper.

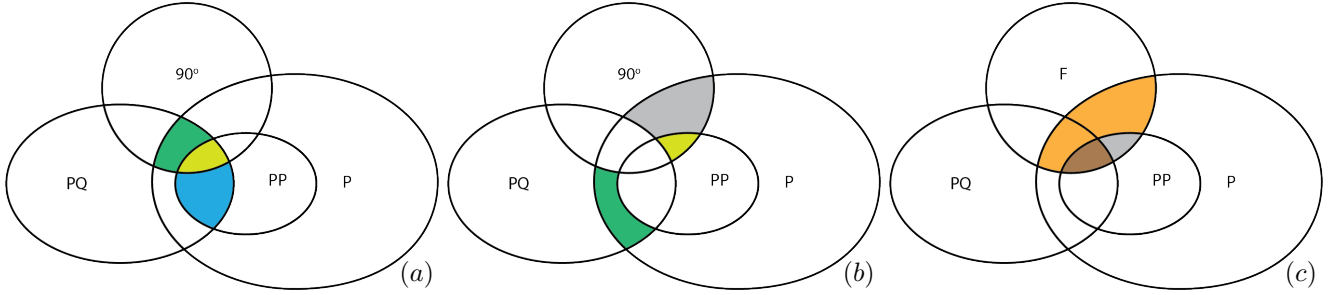


Figure 4: The diagrams show that we work on the combinations of planar parameter lines with other constraints. (a) The colored intersections are studied in the literature [2]. (b) This paper focuses on cases with more general constraints which are not covered in (a). In particular, P+PQ meshes are studied in Section 2 and PP+90° meshes are studied in Section 4. The P+90° meshes constitute a simple case briefly discussed in Subsection 6.3. (c) This paper also investigates the funicularity in meshes of planar parameter lines. PP+PQ+F meshes are studied in Subsection 3.1 and P+(PQ)+F meshes are studied in Subsection 3.2. The PP+F meshes are shortly discussed in Subsection 6.3.

103 possess a relation to translational nets, expressed in terms of
104 projective geometry [2].

105 Another architecturally interesting property is the so-
106 called *funicularity* (or *static equilibrium*), which means that a
107 surface-like structure can resist the load with pure axial forces
108 and has no bending moment. In a self-supporting structure
109 all these axial forces are compressive [12, 13, 14]. Principal
110 meshes in static equilibrium have been studied in [15]. A
111 grid may also admit a self-stressing mode: the internal axial
112 forces that are at equilibrium *without* external load. Such
113 shapes may be realized as a cable-net, a remarkably light-
114 weight structural typology.

115 For architectural construction, it is also useful to have an
116 orthogonal crossing angle of beams at the nodes. This gen-
117 erates repetitive nodes in the whole structure and simplifies
118 the node manufacturing process [16, 17].

119 Planar beams can also be further constrained by consider-
120 ing the plane orientation. Architectural structures can ben-
121 efit from a family of planar supporting beams which are
122 aligned in horizontal, i.e. parallel planes, for example fol-
123 lowing floor slabs. Also, a gridshell with vertical supporting
124 beams can offer a clear top view for a designer and even
125 provide an aesthetic shading pattern, such as in the Dutch
126 Maritime museum [18].

127 The diagrams in Figure 4 show the combinations of con-
128 straints that are covered in this paper.

129 1.3. Contributions and overview

130 In this paper, we present approaches to the computational
131 design of quad meshes with one or two families of planar par-
132 ameter lines with additional properties which play a role in
133 the architectural applications. Specifically, our contributions
134 are as follows:

- In Section 2, we investigate surface approximation by quad meshes with planar parameter lines and planar faces. Since two families of planar parameter lines and face planarity lead to a shape restriction [2], we provide a method for approximating a given surface by a quad mesh with planar faces and one family of planar parameter lines. We also address cases where a global solution does not exist, but one can combine quad meshes with the required properties to a useful global structure with piecewise planar parameter lines.
- In Section 3, we study meshes with planar polylines and funicularity (static equilibrium), with and without considering vertical loads. The former case is interesting from a geometric perspective (Subsection 3.1), the latter is more important for practical design (Subsection 3.2). Using the so-called Airy stress surface, this requires only a small modification of the algorithm presented in Section 2.
- In Section 4, we introduce two methods for finding meshes with planar polylines which meet at an angle of 90°. One approach uses a special class of surfaces with planar orthogonal parameter lines for accessing the design space. The other one starts with a numerical solution of the partial differential equation that needs to be solved in the case of smooth surfaces. In both cases, a global optimization algorithm detailed in Section 5, can be used to modify the initial shapes with mesh editing operations.
- Using the optimization approach described in Section 5, we refine the initialized structures and explore the design space by shape editing. We further provide a number of designs illustrating the capabilities of the presented computational design framework.

1.4. Previous work

Related work on design for fabrication. Meshes with planar polylines have been used in architectural construction and stylized fabrication. Within architectural geometry, we point to work on meshes with planar polylines and planar faces, partially also with a right node angle, based on generation methods which have their origin in classical and constructive geometry [19, 20, 21]. Since a right node angle and planar faces characterize a discrete curvature line parameterization, one has a relation to the classical subject of surfaces with one or both families of planar principal curvature lines. A Laguerre geometric perspective and construction methods based on that have recently been proposed for computational design [2]. We refer to this paper also for a review of the related classical geometric literature.

In addition, we mention research on triangle meshes of regular combinatorics where some or all of the dominant mesh polylines are planar [22].

Besides the constructional advantage for architecture, shapes with planar sections also frequently appear in small- or medium-scale stylized fabrication, for example in artworks called slice-forms [23]. McCrae et al. [24] presented an approach to coarse shape approximation with just a few well-

chosen planar slices, while the interlocked assembly of structures from planar pieces is addressed by Schwartzburg and Pauly [25]. A cross field aligned mesh joinery method was proposed to approximate shapes by several interlocked planar pieces [26]. For more references on stylized fabrication we refer to the survey by Bickel et al. [27].

Related work on smooth surfaces will be described in connection with the respective discrete versions in Sections 2, 3 and 4.

2. Combining planar polylines and planar faces

For many architectural applications, the skin of the structures can be treated as a quad mesh. The edges of the mesh will be part of the support structure and the faces will be panels. There, it is a great advantage if the panels are planar. The resulting planar quad meshes have therefore received a lot of interest in Architectural Geometry (see e.g. [28, 29, 8, 1]).

In this section, we study planar quad (PQ) meshes in which one family of polylines is planar (P+PQ meshes). The generation of PQ meshes with both families of parameter lines being planar (PP+PQ meshes) is restricted in the possible shapes, for which the form-finding methods have been studied in [2].

2.1. Smooth Surfaces

2.1.1. Planar parameter lines

Meshes with planar parameter lines are discrete versions of parameterized surfaces $\mathbf{x}(u, v)$ whose isoparameter lines $u = \text{const}$ and/or $v = \text{const}$ are planar. In this section, we will alternate between the smooth setting and its discrete versions. For some cases, knowledge on the smooth counterparts is important to get insight on the feasibility of certain combinations of constraints. It is also important for an appropriate initialization of the employed optimization algorithms.

In the following, M denotes a quad mesh with grid combinatorics. We consider it parameterized over a rectangular portion of the \mathbb{Z}^2 lattice such that vertex $\mathbf{v}_{i,j}$ is the image of the point $(u, v) = (i, j) \in \mathbb{Z}^2$. The discrete parameter lines belong to constant i or j in the parameter lattice. We are interested in those meshes M for which at least one family of parameter lines is planar. If one or both families of parameter lines are planar, we call the mesh M a *P-mesh* or a *PP-mesh*, respectively.

Our meshes M may be seen as discrete counterparts to smooth surfaces S obtained by a parameterization $\mathbf{x} : \mathbb{R}^2 \supseteq [u_0, u_1] \times [v_0, v_1] \rightarrow \mathbb{R}^3$, whose u -lines ($v = \text{const}$) or/and v -lines ($u = \text{const}$) are planar. The planes in which the u -lines lie are denoted by $U(v)$, and likewise planar v -lines lie in planes $V(u)$. We use the same notation for meshes, but write $U_j = U(j)$ and $V_i = V(i)$ for the planes of parameter lines.

Any surface S can at least locally be parameterized with planar parameter lines. We even have a lot of freedom in prescribing the two families of planes $U(v), V(u)$. However, since we want to achieve a regular parameterization, we have to make sure that the intersection curves $S \cap U(v)$ form a fibration of the surface, and the same shall be true for the

curves $S \cap V(u)$. Moreover, the two curve sets should intersect transversally. This may not be possible globally.

When prescribing the plane families, we have to stay away from the envelope of planes, which is a developable surface that may degenerate to a single straight line (see Fig. 5). Recall that the envelope surface E_U of a family of planes

$$U(v) : u_0(v) + u_1(v)x + u_2(v)y + u_3(v)z = 0,$$

where $u_i(v)$ are C^1 -functions of v , is computed by intersecting the planes with the derivative planes (dots indicating derivatives with respect to v),

$$\dot{U}(v) : \dot{u}_0(v) + \dot{u}_1(v)x + \dot{u}_2(v)y + \dot{u}_3(v)z = 0.$$

The intersection lines $U(v) \cap \dot{U}(v)$ form a developable ruled surface E_U ; for details we refer to [30].

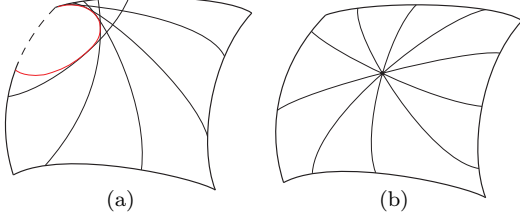


Figure 5: To construct a regular parameterization of a surface with a family of planar parameter lines, one has to avoid the envelope of planes (a). A case which may still be useful despite its singularity is the one where all intersection curves pass through a point (b).

Totally analogous statements hold in the discrete setting. If we would like to approximate a surface S with a P-mesh or PP-mesh M , we have to make sure that the intersection lines of consecutive planes in a family, e.g. $U_j \cap U_{j+1}$ do not intersect the reference surface S .

2.1.2. Conjugate parameterizations

A PQ mesh M approximating a surface S is closely tied to the curvature behavior of S . Assuming that the parameter lines of M are fair and thus represent a proper discretization of a smooth surface parameterization, a PQ mesh M is a *discrete conjugate parameterization* [31, 32]. Hence, it is a discrete counterpart to a conjugate parameterization $\mathbf{x}(u, v)$ of a smooth surface S , that is characterized by linear dependence of the first partial derivatives $\mathbf{x}_u, \mathbf{x}_v$ and the second mixed derivative \mathbf{x}_{uv} . There are infinitely many conjugate parameterizations of a surface S . They are also called *conjugate curve networks*.

To get such a conjugate network one can prescribe one family of curves and get the other family as follows: At each point of S , one computes the conjugate direction to the tangent of the given curve family. This computation can be performed with help of the second fundamental form of $\mathbf{x}(u, v)$ [33]: If $\mathbf{n}(u, v)$ denotes a unit normal vector field of $\mathbf{x}(u, v)$, one forms the inner products with the second derivatives of \mathbf{x} ,

$$L = \mathbf{x}_{uu} \cdot \mathbf{n}, M = \mathbf{x}_{uv} \cdot \mathbf{n}, N = \mathbf{x}_{vv} \cdot \mathbf{n}.$$

Then, two tangent vectors $\mathbf{t}_i = a_i \mathbf{x}_u + b_i \mathbf{x}_v$, $i = 1, 2$ are conjugate if

$$La_1a_2 + M(a_1b_2 + a_2b_1) + Nb_1b_2 = 0. \quad (1)$$

Hence, if one direction is given, we can compute the conjugate direction. Figure 6 uses the *Dupin indicatrix* (radial diagram for $1/\sqrt{|\kappa_n|}$) to illustrate the geometric meaning of conjugate directions as conjugate diameters of the indicatrix. The tangents at the end points of one diameter are parallel to the conjugate diameter. Integration of the field of conjugate directions to the tangents of the first curve family yields the second curve family and thus a conjugate curve network. However, there is a caveat: at hyperbolic points, there are the so-called asymptotic directions (with vanishing normal curvature). They are self-conjugate and therefore have to be avoided if one wants to compute a regular curve network. In fact, for applications one has to avoid small intersection angles between the two curve families as well and thus stay sufficiently far away from asymptotic directions.

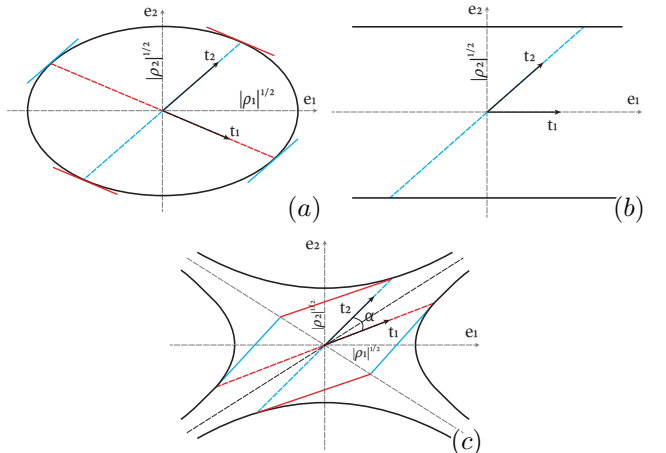


Figure 6: Conjugate directions $\mathbf{t}_1, \mathbf{t}_2$ on the *Dupin indicatrix* in the tangent plane at a point with Gaussian curvature $K > 0$ (a), $K = 0$ (b) and $K < 0$ (c). For $K < 0$, asymptotic directions (asymptotes of the indicatrix) are self-conjugate and conjugate directions close to them form a small angle α

2.2. Approximation with P+PQ meshes

From what has been said above, it is clear that *one can (at least locally) approximate any surface S by a PQ mesh which has one family of planar polylines (P+PQ mesh)*. One has to use a guiding frame field of conjugate parameterization on S in which one tangent vector lies in a family of planes, say $U(v)$. The difficulty arises in areas of negative Gaussian curvature, where one has to choose these planes so that they are nowhere tangent to an asymptotic direction.

2.2.1. Rationalization workflow

We deal with the approximation of a given reference surface S by a P+PQ mesh with regular combinatorics. In architecture, such a process is called rationalization of a design to simplify its fabrication. For a given surface (represented as a dense triangle mesh), we assign a conjugate direction pair to each face barycenter. One direction \mathbf{t}_1 lies in a plane of

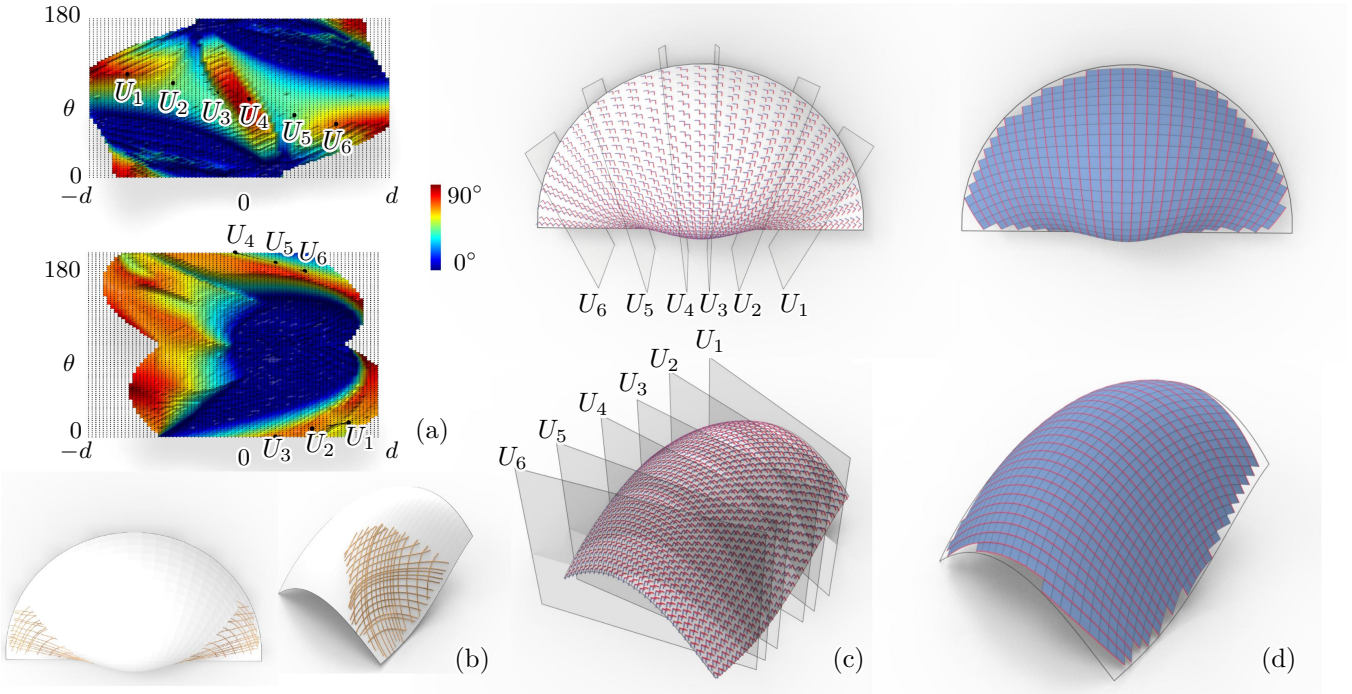


Figure 7: Two examples for approximation with P+PQ meshes. (a) A color-coded quality function is obtained by automatic sampling on the target surface. The user can select vertical planes represented by points on the quality function, noting the periodicity with respect to the angle θ for the consistency and symmetry of planes. (b) The curves on the surfaces show the asymptotic nets as additional support. Chosen planes should not be tangent to asymptotic curves to avoid small angles between conjugate directions. (c) Interpolation of the selected planes and computation of conjugate directions to the intersection curves with the planes yield a conjugate direction field. (d) Based on this conjugate field, we approximate the surface by remeshing and optimization. The red polylines are the planar ones.

315 the family $U(v)$ still to be defined, the other direction \mathbf{t}_2 is
 316 conjugate to it. To compute the conjugate direction, we use
 317 the *jet fit* method of Cazals and Pouget [34] to numerically
 318 calculate the first and second derivatives. The rationalization
 319 workflow is described as below and illustrated in Figure 7.

320 **Selection of planes.** These planes $U(v)$ intersecting the
 321 surface with one family of planar parameter lines should sat-
 322 isfy two conditions:

- 323 • The envelope of the planes should not intersect the sur-
 324 face, as discussed in 2.1.1.
- 325 • The intersecting curve should avoid asymptotic direc-
 326 tions.

327 For initialization, we start with a special case where the
 328 planes containing the parameter lines are vertical. This is an
 329 assumption for structural reasons and can later be changed
 330 in the post-optimization procedure. In a top view, the planes
 331 appear as straight lines. Hence, a proper choice of a family of
 332 planes requires the proper choice of a family of straight lines
 333 in the top view.

334 We provide a color coded quality function as a visual tool
 335 to guide the design of planes. As stated above, planes $U(v)$
 336 are assumed to be vertical (parallel to the z -axis) and of
 337 course have to intersect S . We sample this 2-parameter set
 338 of planes by the signed distance d to the origin (barycenter
 339 of S) and direction angle $\theta \in [0, \pi]$ against the x -axis. Hence,
 340 each possible plane U is represented by a point on the (d, θ)
 341 plane. For each triangle $\Delta_i \subset S$ that intersects U , we take \mathbf{t}_1

342 parallel to the intersection line $\Delta_i \cap U$, compute the conjugate
 343 direction \mathbf{t}_2 and angle α_i between $\mathbf{t}_1, \mathbf{t}_2$. Then the minimal
 344 angle $f(U) = \min(\alpha_i)$ serves as a quality measure for U to
 345 color the corresponding point (d, θ) .

346 The color coded quality function over the (d, θ) -plane
 347 guides the user to select a few good positions for planes
 348 (Fig. 7). In addition, we provide the user with the net of
 349 asymptotic curves (Fig. 7 (b)). Planes have to be selected
 350 so that they are nowhere nearly tangent to an asymptotic
 351 curve. The user-defined planes are then interpolated to ob-
 352 tain a denser set of planes.

353 **Remeshing and optimization.** Based on the selection of
 354 planes, a frame field of pairs of conjugate directions are com-
 355 puted. We re-mesh S by this guiding frame field using the
 356 implementation of mixed integer quadrangulation (MIQ) [35]
 357 in LIBIGL [36]. Using the remeshed structure as an initial-
 358 ization, we employ an optimization procedure to refine the
 359 shape by keeping the essential constraints, such as P, PQ
 360 and proximity to the original shape (see Section 5).

361 2.2.2. Discussion

362 Fig. 7 shows two examples in which the sampling method
 363 helps the user to find initial planes. However, this bound-
 364 ary-to-boundary plane arrangement can fail when the surface has
 365 a complicated behavior of asymptotic directions. For such a
 366 more difficult situation, we can approximate the given shape
 367 by PQ-meshes with one family of piecewise planar polylines.
 368 A solution may incorporate the choice of a combinatorial sin-

369 gularity, for which we do not have an algorithmic solution so
370 far. An example for that is shown by Fig. 8.

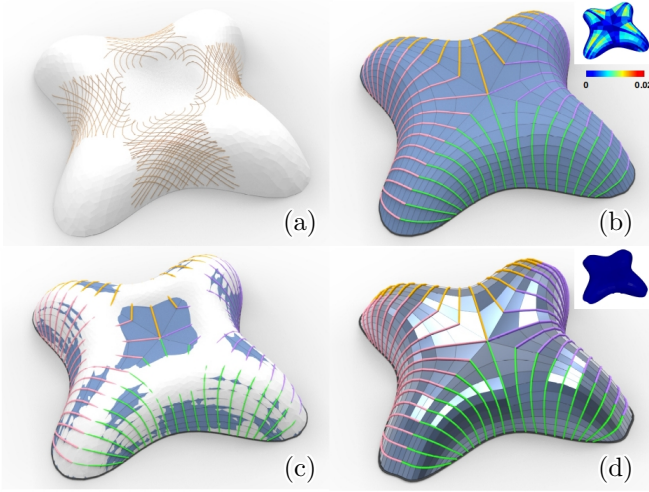


Figure 8: P+PQ mesh approximation for the top of the Lilium Tower. (a) The complicated asymptotic curves lead to no regular settings of planes with good quality. (b) However, we can approximate it by pieces of P+PQ meshes assembled around a central combinatorial singularity of valence 8. One half of the polylines are colored, indicating their planarity in piecewise. In addition, the color-bar shows that the error of face planarity is within the range of 2%, which is measured by the distance between diagonals divided by the average length of diagonals in each face. (c) The optimized P+PQ mesh approximates the input shape well. (d) We can further optimize the faces to be accurately planar at the expense of a larger deviation from the target shape.

3. Combining planar polylines and funicularity

In this section, we combine the constraints of planar polylines and funicularity (static equilibrium) in quad meshes. Static equilibrium has some interesting connections to geometry and it is a natural question for the architectural application. In Subsection 3.1 we discuss equilibrium without external loads, in Subsection 3.2 we consider vertical loads. The former case will be discussed from a geometric perspective, the latter is more important for practical design. Using the so-called Airy stress surface, we link the static equilibrium problem to the planar quad remeshing problem. Hence it requires only a small modification of the algorithm presented in Section 2.

3.1. Static equilibrium without external loads

Initially we deal here only with the case of no external loads, which corresponds for example to the geometry of pre-stressed cable nets.

At first, we consider a supported boundary. Now, each inner edge, for simplicity called $\mathbf{v}_i \mathbf{v}_j$, gets a force density w_{ij} such that $w_{ij}(\mathbf{v}_i - \mathbf{v}_j)$ is the force exerted at \mathbf{v}_i and the opposite force $w_{ij}(\mathbf{v}_j - \mathbf{v}_i)$ is exerted at \mathbf{v}_j . Tensile forces (like in cables) have $w_{ij} < 0$, while compressive forces belong to $w_{ij} > 0$. Equilibrium is characterized by a vanishing resulting force at each inner node \mathbf{v}_i ,

$$\sum w_{ij}(\mathbf{v}_i - \mathbf{v}_j) = 0, \quad (2)$$

where the sum is over all j characterizing the four connected neighbors of \mathbf{v}_i .

For an unsupported boundary, one also has forces in the boundary edges and this condition is applied at the non-supported boundary vertices. This shows the well-known fact that *an unsupported boundary polyline is a discrete asymptotic curve of the surface*: The three edges meeting at an unsupported boundary vertex \mathbf{v}_i must be coplanar and the two boundary edges span the discrete osculating plane of the boundary (see inset in Fig. 9). Now the claim follows from the fact that the osculating planes of an asymptotic curve on a surface are tangent to that surface. The corner vertices, where only two (non-collinear) edges meet, have to be supported; see Figure 9 for an example.

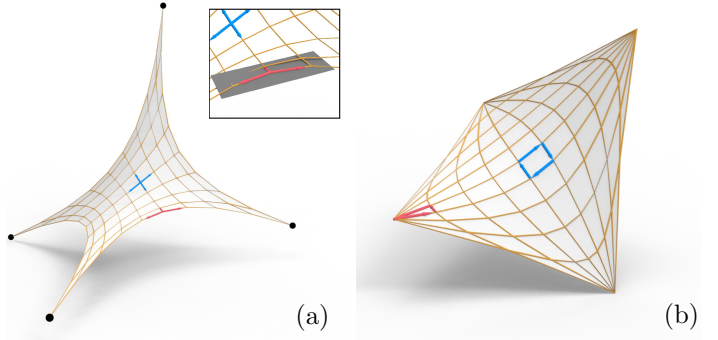


Figure 9: (a) Quad mesh in static equilibrium without external loads, with unsupported boundary and supports only at the four corners. (b) The reciprocal force diagram.

It is a remarkable result that such equilibrium structures are even *invariant under projective transformations* [37]. However, forces and moments have to be transformed like line coordinates. Of course, projective maps also keep the planarity of faces and parameter lines.

According to the principles of graphic statics, one can now form a so-called *reciprocal force diagram*. This is the mesh of forces. Since the forces at a vertex of M sum up to zero, they can be arranged as the edge vectors of a closed quad, and all these quads form the reciprocal mesh M^* . It is known that M^* is also in equilibrium with M as its reciprocal force diagram [38, 37].

Corresponding edges in a reciprocal mesh pair (M, M^*) are parallel. However, edges through a vertex of M belong to edges in a face of M^* and vice versa. One speaks of *reciprocal parallel meshes*. We see that the reciprocal parallel mesh M^* of a PQ mesh M is not a PQ mesh, but a mesh with planar vertex stars, a so-called A-net. A-nets are discrete asymptotic parameterizations and have been studied extensively in discrete differential geometry [31].

Planarity of parameter lines is not preserved when switching from M to M^* . A planar polyline in M (say, in a plane $U(v)$) corresponds to a strip of edges in M^* which are parallel to the plane $U(v)$ and connect the vertices of two neighboring parameter lines of M^* (see Fig. 10). These connecting edges can be viewed as rulings of a so-called conoidal ruled surface.

Hence, the reciprocal mesh M^* to a PP+PQ mesh M in equilibrium (without external forces) is a *discrete affine min-*

imal surface (Fig. 10). It is a discrete version of smooth surfaces which possesses an asymptotic parameterization with the following property: Along each asymptotic curve, the other asymptotic tangents form a conoidal ruled surface (i.e., they are parallel to a plane). According to W. Blaschke [39], this characterizes negatively curved affine minimal surfaces.

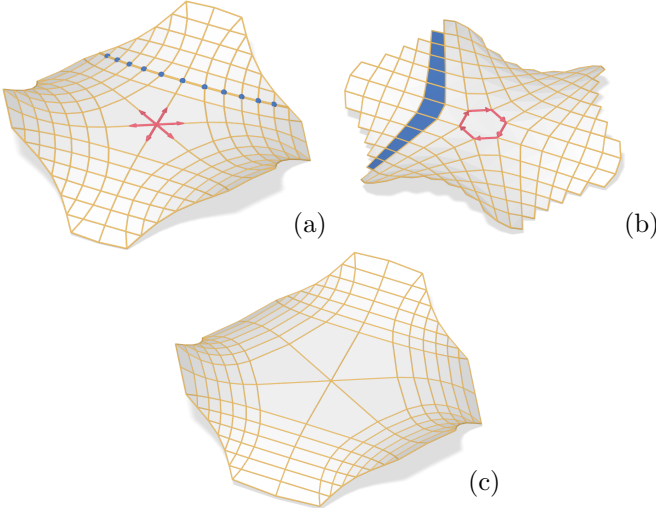


Figure 10: Quad meshes in static equilibrium. (a) A PP+PQ mesh M in static equilibrium. (b) Its reciprocal force diagram M^* is a discrete affine minimal surface. Red: Forces through a vertex of M correspond to edges in a face of M^* . Blue: A planar polyline in M corresponds to a strip of edges in M^* . These edges are parallel to the plane containing the corresponding polyline in M . (c) A parallel mesh \bar{M} of M is also a PQ+PP mesh and in equilibrium with M^* as reciprocal force diagram.

There is another, simpler type of mesh parallelism which plays a role in our context as well. A pair of combinatorially equivalent meshes M, \bar{M} is called parallel (or related by a Combescure transformation [31]) if corresponding edges are parallel. This is only possible for PQ meshes. Since planar parameter lines are also kept under this mesh parallelism, we can state that PQ meshes with planar parameter lines are invariant under mesh parallelism. Obviously, also static equilibrium is preserved under parallelism, since we can take the forces from the original mesh M , i.e., keep the reciprocal force diagram M^* unchanged.

3.2. Static equilibrium with vertical loads

In this subsection, we now consider equilibrium with external loads. We discuss the rationalization of a given shape by a funicular P-mesh (P+F mesh) subjected to vertical loads. It turns out that this approximation task is closely related to the one addressed in 2.2, if we consider the so-called Airy stress surface, explained below.

3.2.1. Airy stress function

As we are dealing with vertical loads, we will project equilibrium along the vertical axis, and introduce the Airy stress function. We recall here some basics about discrete Airy stress functions. A more complete treatment may be found for example in [12].

As shown in Figure 11, for a mesh M in static equilibrium under vertical loads with supported boundary, each unsup-

ported vertex \mathbf{v}_i satisfies an equilibrium equation (assuming a vertical z -axis):

$$\sum w_{ij}(\mathbf{v}_i - \mathbf{v}_j) = \begin{bmatrix} 0 \\ 0 \\ p_i \end{bmatrix}, \quad (3)$$

where the sum is over all j characterizing the connected neighbors of \mathbf{v}_i and p_i is the vertical load on vertex \mathbf{v}_i .

Considering just the x and y coordinates in (3) shows that the top view \bar{M} of M in the xy plane is in equilibrium without external forces and with forces $\bar{\mathbf{f}}_{ij} = w_{ij}(\bar{\mathbf{v}}_i - \bar{\mathbf{v}}_j)$ in the edges. Here $\bar{\mathbf{v}} = (v_x, v_y)$ denotes the top view of a point $\mathbf{v} = (v_x, v_y, v_z)$. The forces $\bar{\mathbf{f}}_{ij}$ at each vertex $\bar{\mathbf{v}}_i$ form a closed planar polygon of the reciprocal force diagram \bar{M}^* . Here we apply a -90° rotation to the force vectors $\bar{\mathbf{f}}_{ij}$ in order to obtain the edge vectors of the force diagram \bar{M}^* .

Based on \bar{M}^* , one can construct a polyhedral mesh (so-called Airy stress surface) $\Phi = (x, y, \phi(x, y))$, which shares the same projection \bar{M} in the xy plane. A planar face f_k of Φ has a gradient $\nabla\phi|_{f_k} = (x_k^*, y_k^*)$ that agrees with the coordinates (x_k^*, y_k^*) of the corresponding vertex $\bar{\mathbf{v}}_k^*$ in the force diagram. Equivalently, the normal vector $\mathbf{n}_k = (n_k^x, n_k^y, n_k^z)$ of face f_k is related to the coordinates of vertex $\bar{\mathbf{v}}_k^*$ by $\bar{\mathbf{v}}_k^* = (n_k^x/n_k^z, n_k^y/n_k^z)$.

We are now considering two faces f_k, f_l of the Airy surface which share a common edge and show how to compute the associated force (horizontal force component in the corresponding edge on M) directly from the Airy surface. Let $\vec{e}_{ij} = (\bar{\mathbf{v}}_i - \bar{\mathbf{v}}_j)/\|\bar{\mathbf{v}}_i - \bar{\mathbf{v}}_j\|$ be the unit vector representing the top view of that edge in the xy -plane. Then, the force along this edge \vec{e}_{ij} is computed by

$$\beta^{is}(\vec{e}_{ij}) = J(\nabla\phi|_{f_k} - \nabla\phi|_{f_l}) \cdot \vec{e}_{ij}, \quad (4)$$

where $J = \begin{bmatrix} 0 & -1 \\ 1 & 0 \end{bmatrix}$ describes the $+90^\circ$ rotation in the xy plane. Note that the difference vector of the gradients $\nabla\phi|_{f_k} - \nabla\phi|_{f_l}$ equals the edge vector in the reciprocal diagram, i.e. the rotated force vector. Reversing the rotation via J and multiplying with the unit edge vector \vec{e}_{ij} gives the force $w_{ij}\|\bar{\mathbf{v}}_i - \bar{\mathbf{v}}_j\|$ with the correct sign. That value is equal to the angle between the planes of faces f_k and f_l , if the angle is measured within isotropic geometry, a simple non-Euclidean geometry which is the appropriate geometric setting in the present context. An introduction to isotropic geometry can be found in [40]. For detailed discussions of the geometry of equilibrium, we refer to [41, 42, 43, 12].

3.2.2. Relation between F and PQ properties

Funicularity, which is a notion that combines geometry and forces, may be expressed as a purely geometrical constraint on the Airy mesh: For a given funicular mesh M and its Airy surface Φ , a funicular quad mesh M_1 representing the discrete surface M corresponds to a PQ mesh that approximates Φ [43, 12]. We will be mainly interested in the reciprocal statement: if we remesh the Airy surface by a PQ mesh Φ_1 , then there is a corresponding funicular mesh M_1 that approximates the design surface M . These statements are precise in the smooth limit. In the present discrete setting, one has degrees of freedom in approximating a given discrete

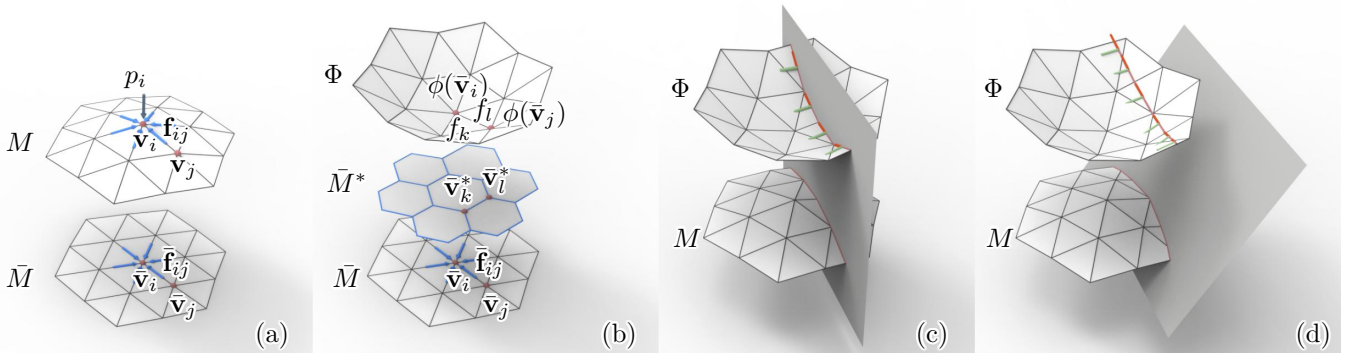


Figure 11: Airy stress surface and using it for remeshing with a P+F mesh. (a) A mesh M in static equilibrium under vertical load with supported boundaries, and its projection \bar{M} onto the xy plane. (b) The horizontal equilibrium of \bar{M} forms a force diagram \bar{M}^* . It is a dual mesh whose edges are constructed from the forces of \bar{M} and rotated by 90 degrees [38]. The Airy polyhedron Φ has the same top view \bar{M} as M . It has planar faces whose gradients are defined by the coordinates of the corresponding vertex of \bar{M}^* . (c) In the special case where M is rationalized towards a P+F mesh with vertical planar polylines, we perform P+PQ remeshing of Φ and map back to M . (d) When the planar polylines on M are not confined to be vertical, we project them in vertical direction to Φ , compute conjugate directions there, and use the resulting cross field on Φ for remeshing.

surface M and an associated polyhedral discrete Airy surface Φ by quad meshes M_1, Φ_1 such that Φ_1 has planar faces. Even when Φ_1 is determined, there is no unique way to compute M_1 . However, the provided geometric relations can be effectively used for initialization of a subsequent optimization which will slightly change the geometrically motivated initial guess and finally achieve the required constraints on the mesh M_1 to be designed, including funicularity, with sufficiently high accuracy.

3.2.3. P+F remeshing

We now propose a method to remesh a funicular triangular mesh M by a P+F mesh.

Firstly, funicularity implies that there exists an Airy stress function Φ . We remark that a polyline of the mesh is in a vertical plane if and only if the corresponding polyline of the Airy polyhedron is in the same vertical plane (Figure 11 (c)). Hence, remeshing M by a P+F mesh (with vertical planar polylines) can be obtained by a P+PQ-remeshing of Φ , followed by a vertical projection of the resulting mesh onto M .

A workflow for P+PQ remeshing was proposed in subsection 2.2. It may be readily used here, applied to the Airy surface instead of being applied directly to the surface. The workflow is particularly simple if Φ is free of asymptotic directions, which happens if all forces are compressive or all are tensile. This is necessary when the structure is a masonry or cable net, respectively. The harder case is the one where both compression and tension occur, since this corresponds to negatively curved regions of the stress surface. The searching with a color-coded function introduced in subsection 2.2 may then be used.

For more general designs, the planar polylines of the P+F mesh need not be vertical. In this case, we have to select planes for the parameter lines on M so that their intersections with the design surface correspond to curves on Φ which avoid asymptotic directions. We then project the planar sections on M vertically to Φ and compute the conjugate field on Φ (Figure 11 (d)). After remeshing the Airy surface Φ according to this conjugate field, it is already close to a PQ mesh. We

can further optimize the face planarity with proximity to the original Airy surface Φ . Then we vertically map the polylines back onto the target M , with the isotropic angle between faces of the Airy mesh as the initial force value. With this initialized mesh and forces, we can find a P+F mesh in close proximity to the given shape by optimization (for details of optimization, see Section 5).

For some special cases where the designed parameter lines are close to the conjugate nets on both Airy surface and target surface, it is possible to rationalize the surface as a P+PQ+F mesh. A self-Airy surface M , which agrees (up to scaling in z -direction) with its Airy surface Φ , is obviously one category of surfaces that can be approximated in this way (Figure 12). As a typical self-Airy surface, paraboloid remarkably combines funicularity with planar faces and polylines [44]. For the construction of self-Airy surfaces, we refer to [42, 43]. Another example of P+PQ+F rationalization is shown in Figure 13. More generally, Figure 14 shows an example of rationalization by a P+F mesh where the Airy surface is not convex, so that remeshing should avoid touching the asymptotic curves.

4. Meshes with orthogonal planar parameter lines

In this section, we combine the constraints of planar polylines with right node angles. We first discuss smooth surfaces with orthogonal planar parameter lines (Subsection 4.1). Accordingly, we introduce two methods for finding meshes with planar polylines which meet at an angle of 90° (Subsection 4.2).

One approach departs from surfaces with parabolas as curves of steepest descent as a special category of surfaces with planar orthogonal parameter lines for accessing the design space. The other one starts with a numerical solution of the partial differential equation that needs to be solved in the case of smooth surfaces. In both cases, a further global optimization as described in Section 5 can be used to edit the meshes.

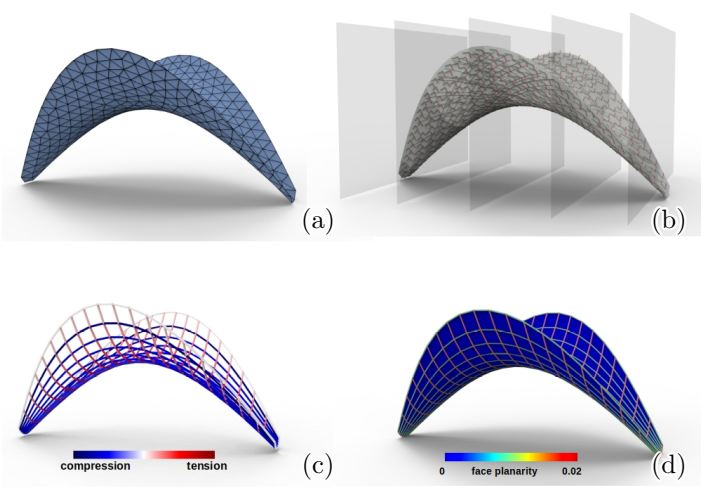


Figure 12: Rationalization of a self-Airy surface by a P+PQ+F mesh. (a) A given self-Airy surface, as shown in [45], is represented by a triangle mesh. (b) Remesh the Airy mesh towards a P+PQ mesh based on the conjugate field guided by the cutting planes. (c) and (d) show the force distribution, planar polylines (actually both families are planar, so we have a PP+PQ+F mesh) and planar quad panels after optimization.

588 4.1. Smooth surfaces

589 Let us first provide a view into classical geometric research
 590 on surfaces which carry two orthogonal families of planar
 591 curves.

592 T. Ivey [46] showed that the only surfaces which carry two
 593 orthogonal families of circles are Dupin cyclides. The circles
 594 are either principal curvature lines or form an angle of 45 degrees
 595 with those (*Villarceau circles*). In the latter case, the
 596 surfaces are related to a Willmore torus (torus of revolution
 597 with radii 1 and $\sqrt{2}$) by a Möbius transformation. The Vil-
 598 larceau circles on other ring cyclides do not intersect under a
 599 right angle, but under a constant angle.

600 Another special case of surfaces with orthogonal planar
 601 parameter lines are those where one family of curves are
 602 straight. These ruled surfaces have been completely classi-
 603 fied by H. Sachs [47]. If they are developable ruled surfaces
 604 and possess a family of curves orthogonal to the rulings, they
 605 are either cylinders or developable surfaces of constant slope.
 606 In both cases the planes $U(v)$ of the curves orthogonal to the
 607 rulings are parallel and thus these are also the surfaces with
 608 straight curves of steepest descent. The surfaces intersect the
 609 planes $U(v)$ under a constant angle. For a detailed study of
 610 these surfaces, we also refer to [30].

611 Generalizations of developable surfaces of constant slope
 612 are surfaces with an orthogonal net of planar curves, where
 613 one family of parameter lines lie in parallel planes. We may
 614 imagine these planes as horizontal. In an architectural ap-
 615 plication they could form the floor slabs of a building. Then
 616 the orthogonal curves are curves of steepest descent. There
 617 has been a number of contributions on surfaces with pla-
 618 nular curves of steepest descent, especially by W. Wunderlich
 619 [48, 49, 50, 51] and more recently by H. Trautwein [52]. If,
 620 in addition the second family of curves lies in vertical planes,
 621 we arrive at the familiar moulding surfaces, which are spe-
 622 cial cases of surfaces with planar curvature lines which have

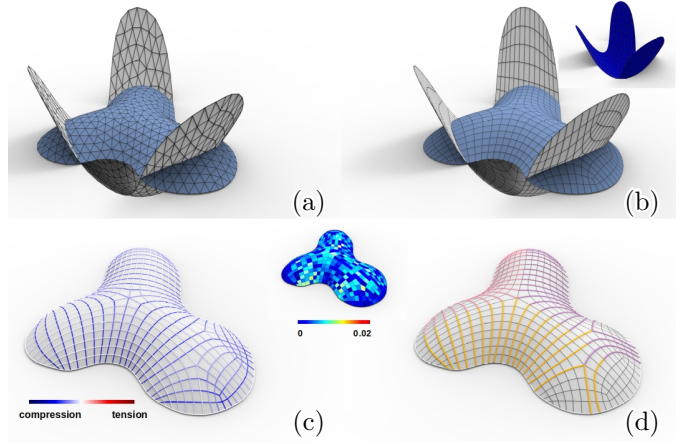


Figure 13: Rationalization with a P+PQ+F mesh. (a) A given surface in static equilibrium (in blue) and its Airy stress surface (in white) are represented by triangle meshes. (b) Design the planes containing planar polylines on the target surface and remesh the Airy mesh along a conjugate field. (c) and (d) show the force distribution, piecewise planar polylines (in colors) and near planar quad panels after optimization.

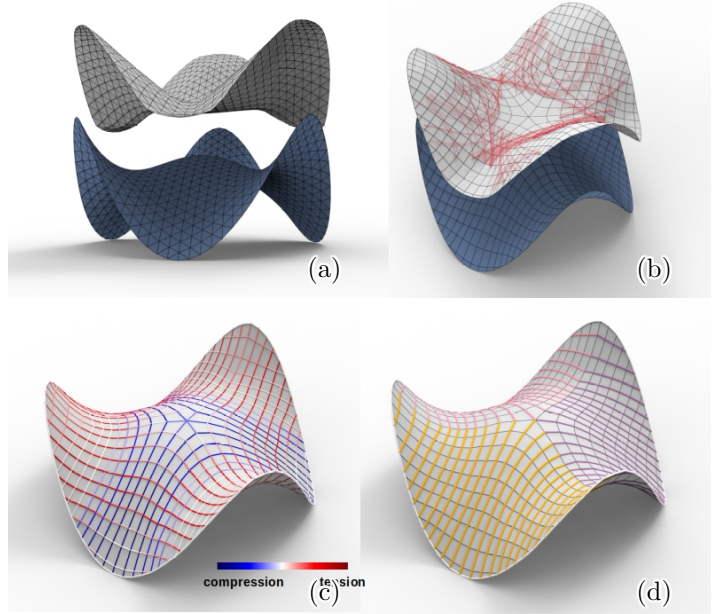


Figure 14: Rationalization with a P+F mesh. (a) A given surface in static equilibrium (in blue) and its Airy stress surface (in white) are represented by triangle meshes. (b) Design the planes containing planar polylines on the target surface and remesh the Airy mesh by a conjugate field without being tangent to the asymptotic curves (in red). (c) and (d) show the force distribution and piecewise planar polylines (in colors) after optimization.

623 recently been discussed in detail in connection with the ar-
 624 chitectural application [19, 20, 2].

625 Surfaces with parabolas as curves of steepest descent. Since our computational approach is based on numerical op-
 626 timization, it is important to have good starting meshes for
 627 further manipulation. In one of the above mentioned papers
 628 on surfaces with planar curves of steepest descent we find a
 629 sufficiently large set of examples to get started with. These
 630 are the surfaces which possess parabolas as curves of steepest
 631

descent. W. Wunderlich [49] provided an elegant construction of all these surfaces through an appropriate transformation of developable surfaces of constant slope (for the latter, see the detailed treatment in [30]). It is sufficient here to assume slope 1. These surfaces Φ^* are envelopes of a one-parameter family of planes which are inclined against the plane $z = 0$ under the angle $\pi/4$:

$$T(v) : x^* \cos v + y^* \sin v - z^* = h(v).$$

Here, the arbitrary function $h(v)$ is the support function of the intersection of Φ^* with the plane $z = 0$. To compute the envelope of tangent planes $T(v)$, we have to compute the derivative planes $\dot{T}(v) : -x^* \sin v + y^* \cos v = \dot{h}(v)$ and intersect with $T(v)$. This yields the developable surface Φ^* of constant slope:

$$\mathbf{x}^*(u, v) = ((h + u) \cos v - \dot{h} \sin v, (h + u) \sin v + \dot{h} \cos v, u).$$

It is convenient to consider complex numbers $\zeta^* = x^* + iy^*$, since then the first two coordinate functions are simply

$$\zeta^* = (h + i\dot{h} + u)e^{iv}.$$

Note that the surface Φ^* has straight u -lines which intersect the v -lines in planes $z = u$ under a right angle. The same right angle appears in the top view (projection into the plane $z = 0$). Following Wunderlich [49], we now apply the conformal map $\gamma : \zeta^* \mapsto \zeta = (\zeta^*)^2$ to the first two coordinates and keep the third coordinate z^* unchanged. This yields the surface Φ :

$$\Phi : \zeta = x + iy = (h + i\dot{h} + u)^2 e^{2iv}, z = u. \quad (5)$$

The conformal map γ transforms straight lines to parabolas with focal point at the origin. The simple 3D extension maps general straight lines in space to parabolas whose axes are parallel to the plane $z = 0$. The v -lines in planes $z = u$ are also transformed by γ and the right angle to the u -lines is preserved. Hence we have a surface Φ all whose curves of steepest descent (u -lines) are parabolas with horizontal axis. Wunderlich shows that the other essentially different case is the one with $z = u^2$ instead of $z = u$. Now all parabolas are tangent to the plane $z = 0$ along a curve and their axes possess constant slope 1. We can set $z = a_0 u^2 + a_1 u$ and also obtain surfaces with parabolas as curves of steepest descent. This amounts to applying the transformation

$$(x^*, y^*, z^*) \mapsto ((x^*)^2 - (y^*)^2, 2x^*y^*, a_0(z^*)^2 + a_1z^*) \quad (6)$$

to Φ^* .

In order to design Φ , it is better to prescribe its curve c in the plane $z = 0$ (see Figures 15). Then, one applies the inverse conformal map $\zeta \mapsto \sqrt{\zeta}$ to it, obtaining a curve c^* on a developable surface Φ^* of constant slope 1. We need not use the support function to compute Φ^* , but just consider the fact that the rulings of Φ^* have the normals of c^* as their top view. Hence, if c^* is given in a parameterization $c^*(v) = (c_1^*(v), c_2^*(v))$, the surface Φ^* can be written as

$$\mathbf{x}^*(u, v) = (c_1^* - \frac{u}{\sqrt{(\dot{c}_1^*)^2 + (\dot{c}_2^*)^2}} \dot{c}_2^*, c_2^* + \frac{u}{\sqrt{(\dot{c}_1^*)^2 + (\dot{c}_2^*)^2}} \dot{c}_1^*, u).$$

Transforming back via a map of the form (6) yields the surface Φ . In the following, surfaces with parabolas as curves of steepest descent will be called *Wunderlich surfaces*.

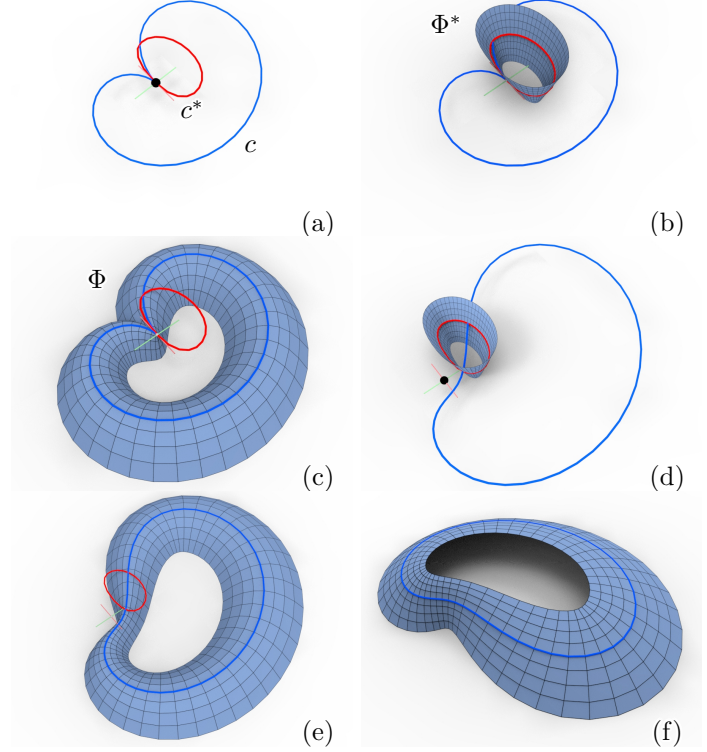


Figure 15: Construction of Wunderlich surfaces. (a) One chooses a curve c (blue) in the plane $z = 0$ and applies the conformal map $\zeta \mapsto \sqrt{\zeta}$ to it. This yields the curve c^* (red). (b) A developable surface Φ^* of constant slope 1 is computed through c^* . (c) Application of a map (6) (here $(a_0, a_1) = (1, 0)$) yields a Wunderlich surface Φ through c . (d,e) The result depends on the location of the origin in the base plane. Here, we fixed c^* and changed the origin. (f) A Wunderlich surface constructed on the same base curve c , but with $(a_0, a_1) = (-0.3, 1)$.

Partial differential equation characterizing surfaces with orthogonal planar parameter lines. Preparing for the construction of orthogonal PP meshes, we first describe here the continuous form. For that, we prescribe two families of planes $U(v), V(u)$ and consider the intersection lines $l(u, v) = U(v) \cap V(u)$. This 2-parameter family of lines (line congruence; see [30]) may be written with a guiding surface $\mathbf{s}(u, v)$ and direction vectors $\mathbf{d}(u, v)$ as

$$l(u, v) : \mathbf{x} = \mathbf{s}(u, v) + w\mathbf{d}(u, v).$$

We have to find $w = w(u, v)$ so that the parameter lines on the surface $\mathbf{x}(u, v) = \mathbf{s}(u, v) + w(u, v)\mathbf{d}(u, v)$ are orthogonal. The orthogonality condition $\mathbf{x}_u \cdot \mathbf{x}_v = 0$ leads to a nonlinear first order PDE for the function $w(u, v)$,

$$(\mathbf{s}_u + w_u \mathbf{d} + w \mathbf{d}_u) \cdot (\mathbf{s}_v + w_v \mathbf{d} + w \mathbf{d}_v) = 0. \quad (7)$$

It is possible to find explicit solutions for special cases such

as the one where both plane families are pencils of planes. However, this would lead too far away from the main purpose of this paper and thus we defer those results to another publication. Here, we focus on the discrete case and note that the construction provided below is an algorithm to find numerical solutions of this PDE.

4.2. Discrete surfaces

We use special quad meshes as discrete models of orthogonal surface parameterizations. As explained in Fig. 16, we require each face in the mesh to have diagonals of equal length. This discrete orthogonality constraint is now used for a numerical solution of equation (7) and later in the global optimization of Section 5.

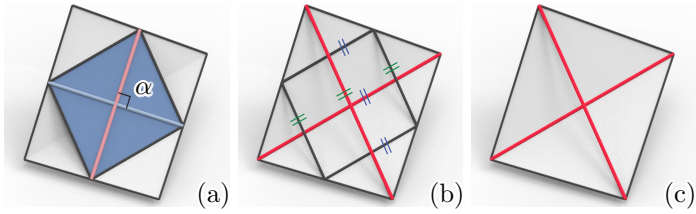


Figure 16: Discrete orthogonal surface parameterizations. (a) Orthogonality is defined per face. In each face, we require orthogonal connecting lines of opposite edge midpoints ($\alpha = 90^\circ$). Edge midpoints are vertices of a parallelogram (blue). Since it has orthogonal diagonals, it is a rhombus. (b) The edges of that rhombus are parallel to the diagonals (red) of the quad and have half of the diagonals length. (c) Hence, discrete orthogonality is formulated via diagonals of equal length in each face of the quad mesh.

4.2.1. Form-finding using propagation for initialization

We are now ready to present a numerical solution of PDE (7) to obtain discrete versions of surfaces with orthogonal planar parameter lines ($PP+90^\circ$ meshes). It is one way to come up with initial shapes that can later be edited by global optimization.

Firstly, we prescribe the planes of parameter lines. One family of parameter lines lie in planes U_1, U_2, U_3, \dots and the other family in planes V_1, V_2, V_3, \dots . This constrains the vertices $\mathbf{v}_{i,j}$ of the mesh to the intersection lines $l_{i,j} = U_i \cap V_j$. In addition to the planarity of parameter lines, we aim at their orthogonality. This requires equal-length diagonals in the quads of the mesh, as shown in Fig. 16.

We can construct a $PP+90^\circ$ mesh to the provided data from one boundary polyline by a *propagation algorithm* as follows: We prescribe a boundary polyline on plane U_1 and an initial guess of the next vertex (green) of the other boundary on plane V_1 as shown in Fig. 17. We can then find the positions of the vertices for the next polyline on plane U_2 via orthogonality. This propagation is achieved by progressively intersecting a sphere (radius equals a known diagonal length) with a line $l_{i,j}$ (Fig. 17 (a)). The number of intersection points can be 2, 1 or 0. If there are two intersection points, we select the one with lower fairness energy (fairness is expressed via 2nd differences; see Section 5). If there is no intersection, it is natural to use the point of $l_{i,j}$ that is closest to the sphere, and thus we get $\mathbf{v}_{i,j}$ by orthogonal projection of the sphere center $\mathbf{v}_{i-1,j-1}$ onto $l_{i,j}$. Immediately after getting

this first version of the mesh polyline in U_2 , we optimize it for fairness keeping the constraints; this will in general change the originally chosen point (green) in V_1 . We then repeat the steps described above to find the next polyline on U_3 , and so on. Finally, we employ a global optimization with various considerations from a practical perspective. This depends on the requirements of the application and may allow deviations from the originally fixed plane positions, from precise discrete orthogonality, and from the boundary in U_1 .

Examples of meshes constructed with the propagation algorithm and later modified through global optimization are shown in Fig. 18. In particular, the figure shows that relaxing the orthogonality constraint enlarges the design space so that further constraints, e.g. at boundaries, can be applied.

4.2.2. Form-finding using Wunderlich surfaces for initialization

A $PP+90^\circ$ mesh with one family of polylines in horizontal planes can be obtained by sampling a Wunderlich surface. Its construction can start from a based curve c , as illustrated in Fig. 15. Sampled Wunderlich surfaces are just a very special subset of $PP+90^\circ$ meshes. They may not fulfil our discrete orthogonality constraint precisely. This does not hurt in the subsequent editing through optimization (see Section 5), which we can apply in order to enlarge the design space. Figs. 19 and 20 show examples.

4.3. Discussion

Both of the proposed methods are suitable for architectural design, as one can easily start with prescribing a base/boundary curve on the ground. The Wunderlich-based initialization has more control on the curves in the steepest descent direction, which however are restricted to parabolas. In contrast, the propagation-based initialization is more flexible, since there is no restriction on the planes carrying the parameter lines. However, propagation is not guaranteed to yield useful results for certain choices of a boundary polyline and planes of parameter lines. Overall, both approaches are able to provide a reasonable initialization for the shape editing with optimization.

5. Optimization

As already mentioned in Sections 2, 3 and 4, numerical optimization is used to refine meshes and to broaden the design space with shape editing. For the computation of constrained meshes, we use the numerical optimization algorithm proposed by Tang et al. [53]. It is an appropriately regularized Gauss-Newton algorithm. An important ingredient for the high performance is the use of constraints that are at most quadratic. In many cases, this can be achieved by the introduction of auxiliary variables. Otherwise, one uses geometrically motivated simplifications and may take certain values for variables from the previous iteration. We do not consider this a main contribution, but just provide the necessary details for a successful implementation.

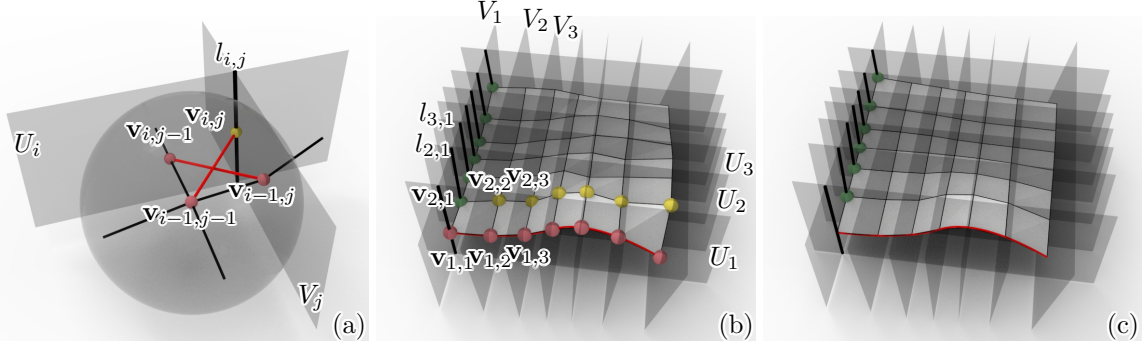


Figure 17: Construction of a PP+90° mesh by propagation. (a) The basic step computes from three known vertices $\mathbf{v}_{i-1,j-1}$, $\mathbf{v}_{i-1,j}$, $\mathbf{v}_{i,j-1}$ to a vertex $\mathbf{v}_{i,j}$ on a line $l_{i,j}$ so that the diagonals in the resulting quad have equal length; this amounts to intersecting a sphere centered at $\mathbf{v}_{i-1,j-1}$ with $l_{i,j}$. (b) Propagation from a prescribed boundary polyline in U_1 to the next polyline in U_2 . (c) Final result after global optimization for fairness.

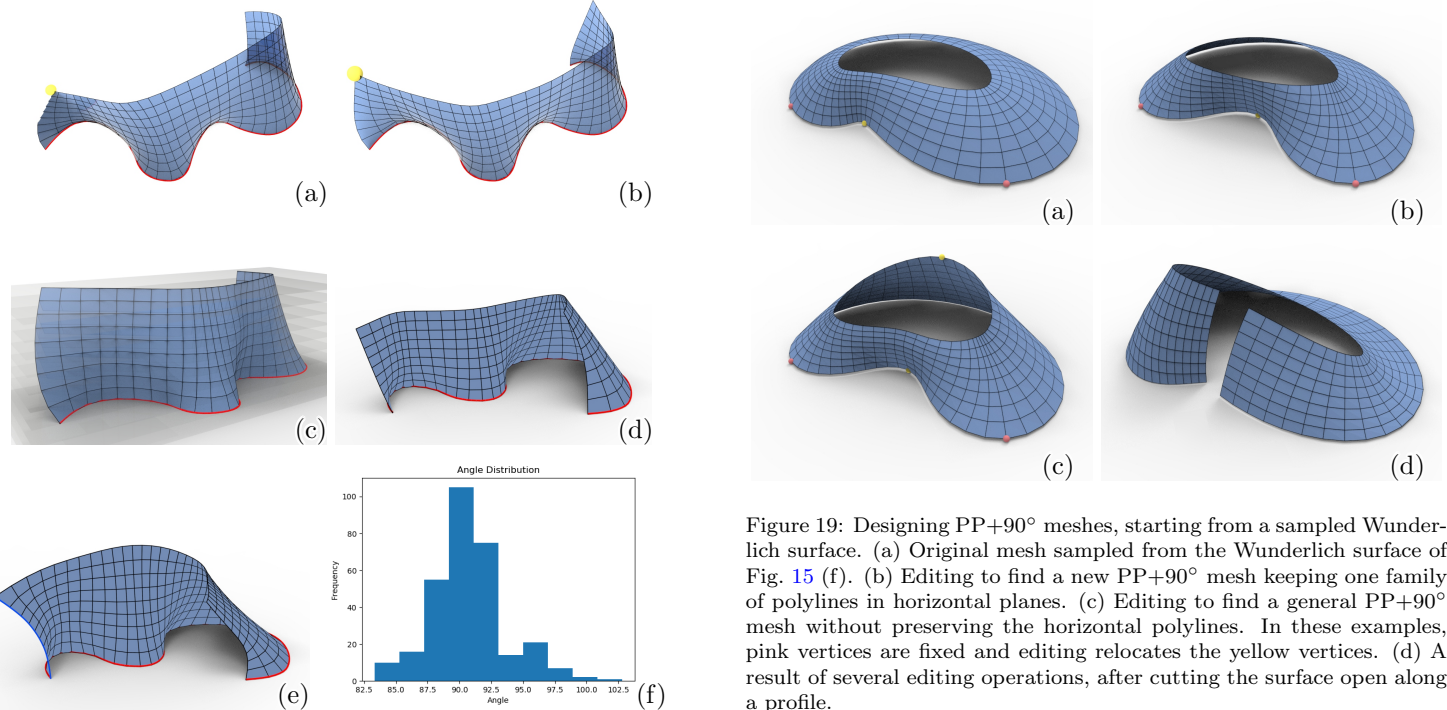


Figure 18: PP+90° meshes found by propagation plus optimization. (a) shows a result of propagation with one prescribed boundary (red) on the ground. (b) The undesirable shape of the surface near the yellow vertex can be improved by changing its position through global optimization keeping the planarity and orthogonality of polylines, the given boundary and fairness. (c) A PP+90° mesh with one family of polylines in horizontal planes, constructed through the same boundary on the ground. (d) Another PP+90° mesh found by propagation plus optimization with a fixed ground boundary. (e) A user may request to control both boundaries (red and blue) for architectural applications. Since a propagation with two fixed boundaries may lose fairness, a soft constraint for orthogonality is applied to find a near orthogonal PP-mesh. (f) shows its angle distribution where the angles are measured between connecting lines of opposite edge midpoints in each face, referring to Fig. 16.

ing optimization \mathbf{n}_p tends to zero and thus the orthogonality constraint is fulfilled in a trivial way, we require a normalized vector \mathbf{n}_p . If p contains l_p vertices, $\mathbf{v}_{p0}, \mathbf{v}_{p1}, \mathbf{v}_{p2} \dots \mathbf{v}_{p,l_p-1}$, this yields the planarity energy

$$E_{PP} = \sum_{p=0}^{|P|-1} \sum_{j=0}^{l_p-2} (\mathbf{n}_p \cdot (\mathbf{v}_{pj} - \mathbf{v}_{p,j+1}))^2 + \sum_{p=0}^{|P|-1} (\mathbf{n}_p \cdot \mathbf{n}_p - 1)^2, \quad (8)$$

where $|P|$ represents the number of polylines in the mesh that need to be planar.

PQ constraints. Analogously, we express planarity of a face i with vertices $\mathbf{v}_{i0}, \mathbf{v}_{i1}, \mathbf{v}_{i2}$ and \mathbf{v}_{i3} as

$$E_{PQ} = \sum_{i=0}^{|F|-1} \sum_{j=0}^3 (\mathbf{n}_i \cdot (\mathbf{v}_{ij} - \mathbf{v}_{ik}))^2 + \sum_{i=0}^{|F|-1} (\mathbf{n}_i \cdot \mathbf{n}_i - 1)^2, \quad (9)$$

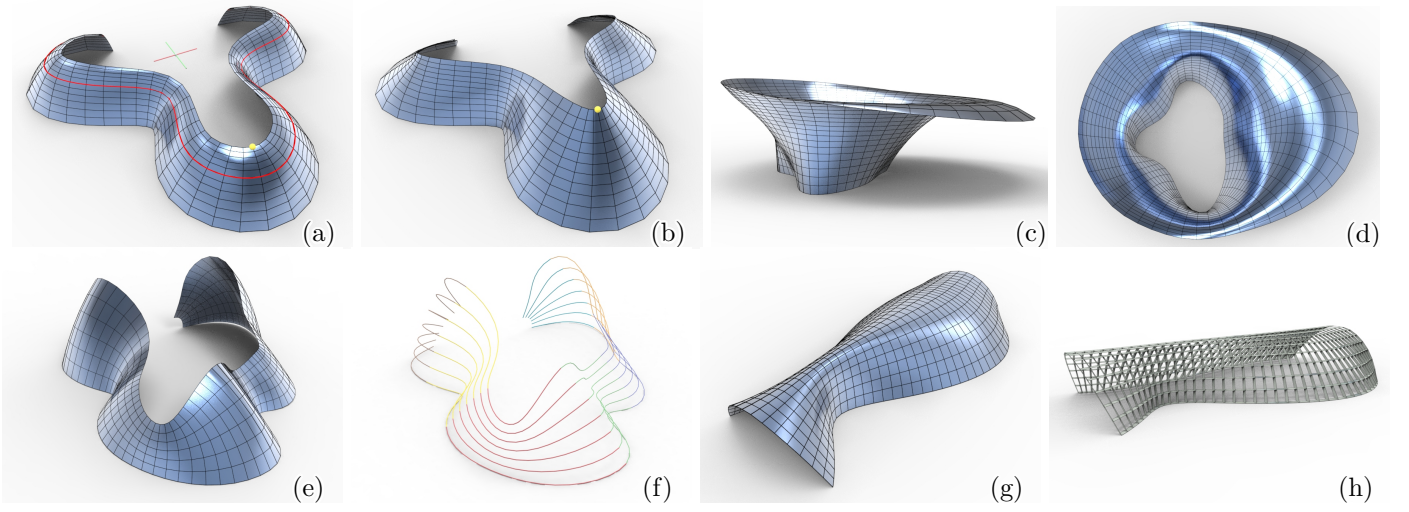


Figure 20: PP+90° meshes designed via editing Wunderlich surfaces. (a) Sampled Wunderlich surface, designed through the red curve. (b) A PP+90° mesh obtained from (a) by fixing the bottom boundary and lifting the yellow vertex. (c) and (d) show a design obtained by editing a Wunderlich surface through a user-defined bottom curve. (e) The design freedom is enlarged by requiring one family of parameter lines to be just piecewise planar; the pieces are colored in (f). (g) shows another design and its support structures from planar long-range beams in (h).

where $|F|$ denotes the number of faces in the mesh and index $k \equiv j + 1 \pmod{4}$.

Orthogonality constraints. As discussed in 4.2, discrete orthogonality of a face i requires diagonals of equal length, leading to

$$E_{orth} = \sum_{i=0}^{|F|-1} (\|\mathbf{v}_{i2} - \mathbf{v}_{i0}\|^2 - \|\mathbf{v}_{i3} - \mathbf{v}_{i1}\|^2)^2. \quad (10)$$

Static equilibrium constraints. Following up on Section 3, we provide a generalized energy term of static equilibrium with vertical loads on vertices. Each unsupported vertex \mathbf{v}_i in the quad mesh has adjacent vertices that form a set V_i . For each $\mathbf{v}_j \in V_i$, we introduce a force density w_{ij} as in Eq. (2). We assume the vertical load (along z-axis) on vertex \mathbf{v}_i is p_i , and thus force balance yields

$$E_{static} = \sum_{i=0}^{|V|-1} \left(\sum_{j:\mathbf{v}_j \in V_i} w_{ij}(\mathbf{v}_i - \mathbf{v}_j) - \begin{bmatrix} 0 \\ 0 \\ p_i \end{bmatrix} \right)^2, \quad (11)$$

where $|V|$ represents the number of unsupported vertices in the quad mesh. In Figure 13 and 14, p_i represents a uniformly distributed area load on vertices considering the barycentric area around vertex \mathbf{v}_i .

Fairness constraints. The fairness term is based on second order differences of mesh polylines and the graph Laplacian. For a vertex \mathbf{v}_i which is not on the boundary, its immediate neighbours are $\mathbf{v}_{i0}, \mathbf{v}_{i1}, \dots, \mathbf{v}_{i,n-1}$. The fairness energy of the mesh is calculated by Eq. (12) for regular vertices (valence equal to 4) and Eq. (13) for irregular vertices (valence $n \neq 4$):

$$E_{fairness} = \sum_{i=0}^{|V|-1} \left(\mathbf{v}_i - \frac{\mathbf{v}_{i0} + \mathbf{v}_{i2}}{2} \right)^2 + \left(\mathbf{v}_i - \frac{\mathbf{v}_{i1} + \mathbf{v}_{i3}}{2} \right)^2, \quad (12)$$

$$E_{fairness} = \sum_{i:\mathbf{v}_i \in singularities} \left(\mathbf{v}_i - \frac{\mathbf{v}_{i0} + \dots + \mathbf{v}_{i,n-1}}{n} \right)^2. \quad (13)$$

Proximity constraints. In the mesh approximation tasks, proximity terms are applied to constrain the mesh vertices to be close enough to the target shape. We use two types of proximity constraints in this paper, expressing squared distances to closest points and to tangent planes at closest points, respectively. The latter has more weight and is known to be a good approximation of the squared distance function of a surface at points near that surface [54]. Given a vertex \mathbf{v}_i , we use a KD-Tree based searching method to find its closest point $\mathbf{v}_{i,ref}$ on the reference surface (represented by a dense triangle mesh). Then the proximity term is calculated by Eq. (14) for point distance or/and by Eq. (15) for tangent distance, in which we introduce the normal vector $\mathbf{n}_{i,ref}$ at $\mathbf{v}_{i,ref}$ on the reference surface,

$$E_{prox} = \sum_{i=0}^{|V|-1} (\mathbf{v}_i - \mathbf{v}_{i,ref})^2, \quad (14)$$

$$E_{prox_tan} = \sum_{i=0}^{|V|-1} ((\mathbf{v}_i - \mathbf{v}_{i,ref}) \cdot \mathbf{n}_{i,ref})^2. \quad (15)$$

5.2. Optimization parameters

With the constraints mentioned above, we arrive at an objective function E_{total} :

$$E_{total} = \lambda_1 E_{PP} + \lambda_2 E_{PQ} + \lambda_3 E_{angle} + \lambda_4 E_{static} + \lambda_5 E_{fairness} + \lambda_6 E_p \quad (16)$$

where λ_5 should be lower than other parameters in an order of magnitude as a “soft” constraint. We solve this optimization problem by a Levenberg-Marquardt method with a fixed damping parameter 10^{-6} . The specific parameters we used for selected figures are listed in Table 2.

It is useful to mention such details: Within the iterations, the energy terms of the constraints that need to be fulfilled such as E_{PP} , E_{PQ} , E_{angle} and E_{static} can be optimized to a value lower than 10^{-3} (the meshes are standardized to the scale with an average edge length equal to 1). We further check the planarity δ_f of faces by the distance of diagonals divided by average length of diagonals, which has a typical value lower than 10^{-4} . Similarly, we check the planarity δ_P of polyline P which is the maximum distance of P ’s vertices from a best approximating plane, divided by the bounding box diameter of P . The typical value of δ_P is lower than 10^{-3} .

6. Extended results and discussion

6.1. P+PQ meshes

In subsection 2.2, we discussed surface approximation by P+PQ meshes initialized with vertical planar beams. Here, we illustrate more broadly the freedom in the design of P+PQ meshes.

Fig. 21 (a) shows an optimization result of a P+PQ mesh with vertical planar polylines. However, when the topology of the mesh is not regular, it will be no longer possible to keep all the polylines in vertical planes. In this case, we could still achieve planes intersecting the ground at angles close to 90 degrees (Fig. 21 (b)).

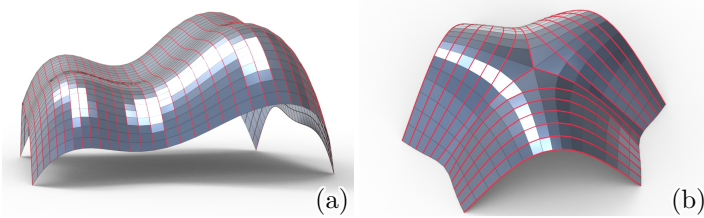


Figure 21: Design of P+PQ meshes. (a) A P+PQ mesh with vertical planar polylines. The vertical planar polylines are colored in red. (b) A P+PQ mesh designed with a combinatorial singularity. Only the planar polylines emanating from the singularity are vertical, others are on nearly vertical planes.

Furthermore, we discuss an example for a targeted choice of plane directions for the planar polylines. The planes can be chosen in order to control the amount of sunlight passing through the support structure. In Fig. 22, we illustrate shading patterns at different times in a day. There, the application is not shading, but we let enough light pass through the structure. This is done by choosing a sequence of planes for the planar polylines in which each plane is parallel to the incoming light at different times of the day. To achieve maximal shading, one needed to position the planes as orthogonal as possible to the sun light. For a discussion of this and related aspects, we refer to Wang et al. [55]. However, that paper does not have planar parameter lines and thus the fabrication of the support structure would be more complicated.

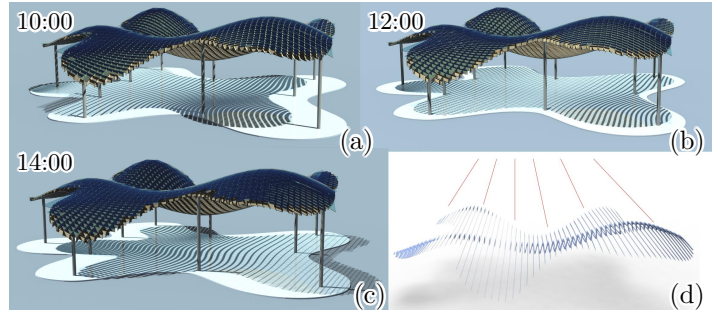


Figure 22: A P+PQ mesh with its support structure generates different shading patterns during a day. (d) illustrates the front view of the support structure aligned with the family of planar polylines. The red lines indicate selected plane positions. When the light is parallel to those, the respective parts in the shading pattern are lighter, well seen in (a-c).

In order to achieve more design freedom, we can consider meshes where every N -th polyline in a family is planar. One will then place the main load-carrying beams of the structure in those planes. As for the Strasbourg train station (Fig. 3 (c)), these planar beams are the primary load-bearing structures reinforced by the “bike-wheel” cables. Fig. 23 shows the design of a PQ mesh in which every fifth polyline in one family is planar.

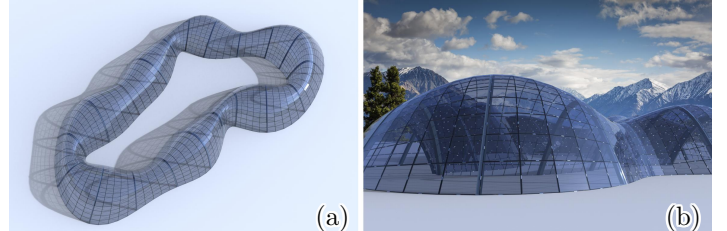


Figure 23: A PQ mesh in which every fifth polyline of a family is planar. Along these polylines the main load-carrying and stabilizing beams of the structure are placed.

6.2. PP+90° meshes

In Section 4, we introduced two initialization methods for the design of PP+90° meshes, whose shapes can be further edited by optimization. Fig. 24 shows more architectural designs of PP+90° meshes initialized by Wunderlich surfaces with a prescribed base curve on the ground. One can observe that for such combination of constraints, we ask for the orthogonality of the crossing angles of planar polylines rather than the orthogonality of the planes of the support structure. An important advantage lies in repetitive nodes. These are not directly present in our discrete versions. However, it is straightforward to represent each planar parameter line by a smooth curve, e.g. a C^1 cubic spline, so that the arising curve network has precise orthogonal node angles (see Fig. 25).

It is important to mention that accessing the design space through a proper choice of initial shapes is important. Fig. 26 shows an example. Looking for a PP+90° mesh, one may have the idea to start with a PP mesh approximating the desired shape and then optimize for orthogonality, maybe even

Fig.	V	F	#var	#cons	λ_1	λ_2	λ_3	λ_4	λ_5	λ_6	λ_7	#iterations	time[s]/it
8(b)	881	800	5202	13284	1	1	0	0	0.15	0	0.3	10	0.89
8(d)	881	800	5202	12403	1	5	0	0	0.1	0.1	0	10	0.85
13(d)	557	503	4425	7989	1	1	0	1	0.02	0.1	0.2	10	0.63
14(d)	728	655	3803	9351	1	0	0	1	0.1	0.2	0.3	10	0.74
18(a)	350	306	1185	2836	1	0	1	0	0.15	0	0	30	0.49
18(b)	350	306	1185	2836	1	0	1	0	0.1	0	0	10	0.37
18(c)	350	306	1185	2856	1	0	1	0	0.1	0	0	10	0.38
18(d)	350	306	1185	2836	1	0	1	0	0.1	0	0	10	0.45
18(e)	350	306	1185	2836	1	0	0.1	0	0.1	0	0	10	0.37
20(b)	600	539	1986	4967	1	0	1	0	0.03	0	0	10	0.73
20(c)	1071	1020	3429	9282	1	0	1	0	0.03	0	0	10	0.88
20(e)	588	498	2163	4698	1	0	1	0	0.03	0	0	10	0.62
20(g)	640	585	2088	5401	1	0	1	0	0.15	0	0	10	0.39
21(a)	1225	1156	7248	13970	1	1	0	0	0.03	0	0	10	0.92
21(b)	331	288	1923	3531	1	1	0	0	0.05	0	0	10	0.45
22	6241	6084	37212	98123	1	1	0	0	0.1	0.1	0	10	6.51
23	2100	2000	12360	24520	1	1	0	0	0.1	0	0.1	10	1.82

Table 2: This table gives an overview of the size of optimization problems solved for various examples in this paper. We also provide the parameter settings and computation time in seconds. The algorithms are implemented in Python and tested on the CPU processor with Intel Xeon CPU E5-2697 2.60GHz.

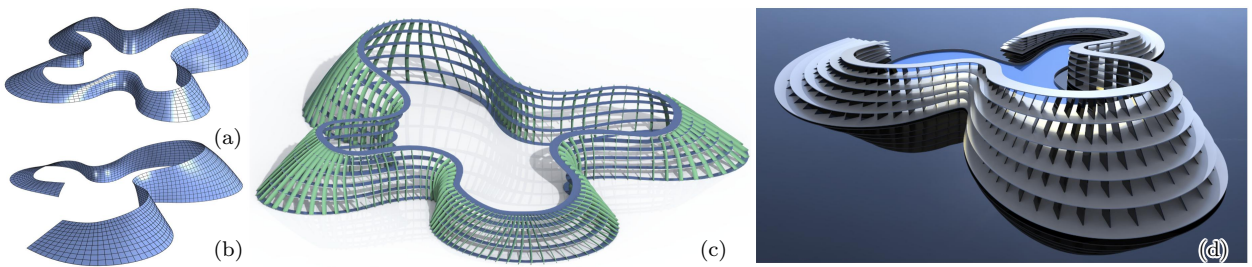


Figure 24: Two PP+90° meshes (a),(b) and corresponding renderings highlighting the planes of supporting structures (c),(d).

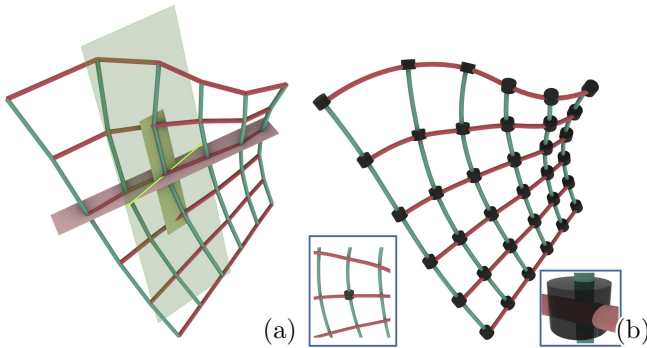


Figure 25: Right node angle and repetitive nodes. (a) A free-form PP+90° mesh has supporting planes which are in general not orthogonal, and the edges do not meet in the nodes at precise right angles. (b) The mesh can be turned into a network of planar smooth curves with precise 90° crossing angles at nodes. One can fabricate it as a network of long-range continuous planar beams, where one family is stacked on top of the other and fixed by a repetitive node with a right node angle.

faces in our case) and then navigates in that space by editing operations.

6.3. Feasible constraints

We have shown the feasible combinations of constraints in quad meshes with planar parameter lines. For a further discussion, these combinations are classified into two tasks, approximation or form-finding, according to their shape restrictions (See Table 3). The former can at least locally approximate a given surface, but the latter is restricted to special shapes. Here we point out that the approximation task with P+90° meshes can be easily achieved by intersecting the target surface with a family of planes which contain the parameter lines and remeshing on the corresponding orthogonal fields, taking Subsection 2.2 as a reference. For the form-finding task of PP+F meshes, one can take a P+F mesh and its respective force density as initialization, then it would be possible to find the very restricted PP+F meshes with shape deviation through optimization.

7. Conclusion and future research

In this article, we investigated the design space of meshes with planar polylines in the presence of additional constraints. We provided a solution for approximating a given

closeness to the original shape. The figure illustrates that such an approach is likely to fail. In general, the more constrained a mesh is, the more care has to be taken in choosing initial shapes. Ideally, one accesses the design space through shapes which already fulfil all constraints (Wunderlich sur-

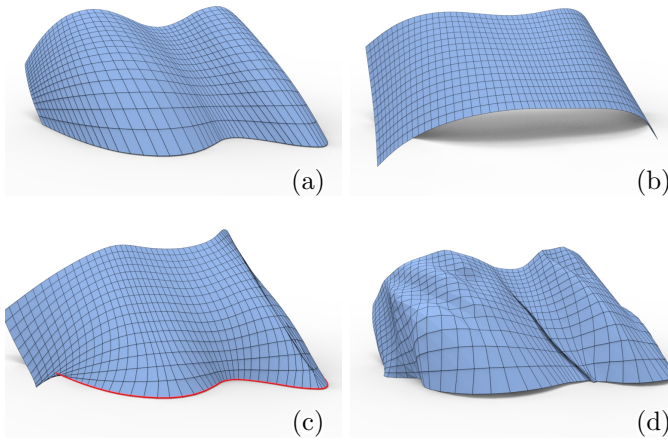


Figure 26: A straightforward approach to PP+90° meshes via optimization based on initialization with a non-orthogonal PP-mesh is problematic. (a) A general PP-mesh as initialization. (b) Directly optimizing for right node angles while preserving planarity generates a trivial result with a big shape change. (c) Optimization with a fixed boundary (red) on the ground fails in searching for useful plane directions. (d) Optimization with a closeness constraint to the original shape results in bad fairness.

Combinations	P-mesh	PP-mesh
PQ	Approximation	Form-finding
90°	Approximation	Form-finding
PQ+90°	Form-finding	Form-finding
F	Approximation	Form-finding

Table 3: An overview of the constraint combinations in quad meshes with planar polylines. The constraint combinations are either discussed in this paper (red) or in [2] (blue).

surface by a P+PQ mesh. Also, we considered meshes with planar polylines in static equilibrium, without vertical load from the geometric perspective, as well as with vertical load for the architectural rationalization. In addition, we introduced two initialization methods for PP+90° meshes, and used optimization-based editing to explore the shape space. Finally, we provided details on our computational framework and illustrated its capabilities by a number of examples. The results show that long-range planar beams provide clear advantages for manufacturing, but appear to have structural benefits as well.

Directions for future research include automatic solutions for the approximation problem with P+PQ meshes, especially when a global solution has to use piecewise planar parameter lines. We also did not yet provide a general strategy for the design of P+PQ+F meshes. In our paper, Wunderlich surfaces turned out to be very helpful for the design of PP+90° meshes. Therefore, one would expect great benefits from explicit solutions of the PDE (7). We have already made some progress in this direction and hope to present sufficiently large and practically useful classes of surfaces with an orthogonal family of planar parameter lines in the near future.

Acknowledgements

This research has been supported by KAUST baseline funding (grant BAS/1/1679-01-01). We are very grateful to Davide Pellis and Yu-Chou Chiang for sharing Airy stress surfaces and valuable discussion on static equilibrium.

References

- [1] H. Pottmann, M. Eigensatz, A. Vaxman, J. Wallner, Architectural geometry, Computers and Graphics 47 (2015) 145–164.
- [2] C. Jiang, C. Wang, X. Tellier, J. Wallner, H. Pottmann, Planar panels and planar supporting beams in architectural structures, ACM Trans. Graph. Just Accepted. doi:10.1145/3561050. URL <https://doi.org/10.1145/3561050>
- [3] S. McCormick, C. Besjak, D. S. Korista, W. Baker, Schubert club band shell, saint paul, minnesota, usa, Structural Engineering International 14 (2) (2004) 140–141. doi:10.2749/101686604777963982. URL <https://doi.org/10.2749/101686604777963982>
- [4] W. Sobek, L. Blandini, The Mansuetu Library - Notes on a glazed steel grid shell from design to construction, Challenging Glass 2 - Conference on Architectural and Structural Applications of Glass, CGC 2010 (May) (2010) 179–185.
- [5] V. Schmid, J. P. Koppitz, A. Thurik, Neue Konzepte im Holzbau mit Furnierschichtholz - Die Holztragkonstruktion des Metropol Parasol in Sevilla, Bautechnik 88 (10) (2011) 707–714. doi:10.1002/bate.201101508.
- [6] H. Schober, Transparent Shells: Form, Topology, Structure, Ernst & Sohn, 2015.
- [7] K. Mam, Exploration structurelle et environnementale des ouvrages en bois de grande portée, Phd thesis, Ecole des Ponts Paris-Tech (2021). URL <https://pastel.archives-ouvertes.fr/tel-03572887>
- [8] H. Pottmann, Y. Liu, J. Wallner, A. Bobenko, W. Wang, Geometry of multi-layer freeform structures for architecture, ACM Trans. Graph. 26 (3) (2007) 65–es. doi:10.1145/1276377.1276458. URL <https://doi.org/10.1145/1276377.1276458>
- [9] N. Baldassini, H. Pottmann, J. Raynaud, A. Schiftner, New Strategies and Developments in T ransparent Free-Form Design : From Faceted to Nearly Smooth Envelopes, International Journal of Space Structures 25 (3) (2010) 185–197.
- [10] J. Schlaich, H. Schober, Glass-Covered Grid-Shells, Structural Engineer (1996) 88–90.
- [11] X. Tellier, C. Douthe, L. Hauswirth, O. Baverel, Funicularity of conics, Acta Mechanica 232 (8) (2021) 3179–3191. doi:10.1007/s00707-021-02987-6. URL <https://doi.org/10.1007/s00707-021-02987-6>
- [12] E. Vouga, M. Höbinger, J. Wallner, H. Pottmann, Design of self-supporting surfaces, ACM Trans. Graph. 31 (4). doi:10.1145/2185520.2185583. URL <https://doi.org/10.1145/2185520.2185583>
- [13] L. Ma, Y. He, Q. Sun, Y. Zhou, C. Zhang, W. Wang, Constructing 3d self-supporting surfaces with isotropic stress using 4d minimal hypersurfaces of revolution, ACM Trans. Graph. 38 (5). doi:10.1145/3188735. URL <https://doi.org/10.1145/3188735>
- [14] L. Ma, S. Yao, J. Zheng, Y. Liu, Y. Zhou, S.-Q. Xin, Y. He, Constructing self-supporting surfaces with planar quadrilateral elements, Computational Visual Media (2022) 1–13.
- [15] D. Pellis, H. Pottmann, Aligning principal stress and curvature directions, in: Advances in Architectural Geometry, 2018.
- [16] E. Schling, Repetitive structures, Ph.D. thesis, Chair of Structural Design, Technical University of Munich, DOI: 10.14459/2018md1449869 (2018). URL <https://doi.org/10.14459/2018md1449869>
- [17] C. Jiang, C. Wang, E. Schling, H. Pottmann, Computational design and optimization of quad meshes based on diagonal meshes, in: Advances in Architectural Geometry Conference (AAG 2020), 2021.
- [18] S. Adriaenssens, M. Asce, L. Ney, E. Bodarwe, C. J. Williams, Finding the Form of an Irregular Meshed Steel and Glass Shell

- 1028 Based on Construction Constraints, Journal of Architectural En- 1103
1029 gineering 18 (September) (2012) 206–213. doi:[10.1061/\(ASCE\)AE.1943-5568.000074](https://doi.org/10.1061/(ASCE)AE.1943-5568.000074). 1104
1030 [19] R. Mesnil, C. Douthe, O. Baverel, B. Léger, Morphogenesis of 1105
1031 surfaces with planar lines of curvature and application to archi- 1106
1032 tectural design, Automation in Construction 95 (2018) 129–141. 1107
1033 doi:[10.1016/j.autcon.2018.08.007](https://doi.org/10.1016/j.autcon.2018.08.007). 1108
1034 [20] X. Tellier, Morphogenesis of curved structural envelopes under fab- 1109
1035 rication constraints, Ph.D. thesis, Univ. Paris-Est (2020). 1110
1036 [21] X. Tellier, C. Douthe, L. Hauswirth, O. Baverel, Surfaces with pla- 1111
1037 nar curvature lines: Discretization, generation and application to 1112
1038 the rationalization of curved architectural envelopes, Automation 1113
1039 in Construction 106. doi:<https://doi.org/10.1016/j.autcon.2019.102880>. 1114
1040 [22] B. Deng, H. Pottmann, J. Wallner, Functional webs for freeform ar- 1115
1041 chitecture, Computer Graphics Forum 30 (2011) 1369–1378, proc. 1116
1042 Symp. Geometry Processing. 1117
1043 [23] J. Sharp, Sliceforms, Norfolk, UK: Tarquín Publications. 1118
1044 [24] J. McCrae, K. Singh, N. J. Mitra, Slices: A shape-proxy based 1119
1045 on planar sections, ACM Trans. Graph. 30 (6) (2011) 1–12. doi: 1120
1046 10.1145/2070781.2024202. 1121
1047 URL <https://doi.org/10.1145/2070781.2024202> 1122
1048 [25] Y. Schwartzburg, M. Pauly, Fabrication-aware design with inter- 1123
1049 secting planar pieces, Wiley Online Library. 1124
1050 URL <https://onlinelibrary.wiley.com/doi/full/10.1111/cgf.12051> 1125
1051 [26] P. Cignoni, N. Pietroni, L. Malomo, R. Scopigno, Field-aligned 1126
1052 mesh joinery, ACM Trans. Graph. 33 (1). doi:[10.1145/2537852](https://doi.org/10.1145/2537852). 1127
1053 URL <https://doi.org/10.1145/2537852> 1128
1054 [27] B. Bickel, P. Cignoni, L. Malomo, N. Pietroni, State of the art on 1129
1055 stylized fabrication, Computer Graphics Forum 37 (6) (2018) 325– 1130
1056 342. doi:<https://doi.org/10.1111/cgf.13327>. 1131
1057 URL <https://onlinelibrary.wiley.com/doi/abs/10.1111/cgf.13327> 1132
1058 [28] Y. Liu, H. Pottmann, J. Wallner, Y.-L. Yang, W. Wang, Geomet- 1133
1059 ric modeling with conical meshes and developable surfaces, ACM 1134
1060 Trans. Graphics 25 (3) (2006) 681–689. 1135
1061 [29] R. Mesnil, C. Douthe, O. Baverel, B. Léger, Marionette meshes: 1136
1062 modelling free-form architecture with planar facets, International 1137
1063 Journal of Space Structures 32 (3-4) (2017) 184–198. 1138
1064 [30] H. Pottmann, J. Wallner, Computational Line Geometry, Springer, 1139
1065 2001. 1140
1066 [31] A. I. Bobenko, Y. B. Suris, Discrete differential geometry. In- 1141
1067 tegrable structure, Vol. 98 of Graduate Studies in Mathematics, 1142
1068 American Mathematical Society, Providence, RI, 2008. 1143
1069 [32] Y. Liu, W. Xu, J. Wang, L. Zhu, B. Guo, F. Chen, G. Wang, 1144
1070 General planar quadrilateral mesh design using conjugate direc- 1145
1071 tion field, ACM Trans. Graph. 30 (6) (2011) 1–10. doi:[10.1145/2070781.2024174](https://doi.org/10.1145/2070781.2024174). 1146
1072 URL <https://doi.org/10.1145/2070781.2024174> 1147
1073 [33] M. do Carmo, Differential Geometry of Curves and Surfaces, 1148
1074 Prentice-Hall, 1976. 1149
1075 [34] F. Cazals, M. Pouget, Estimating differential quantities using 1150
1076 polynomial fitting of osculating jets, Vol. 22, 2003, pp. 177–187. 1151
1077 doi:[10.1016/j.cagd.2004.09.004](https://doi.org/10.1016/j.cagd.2004.09.004). 1152
1078 [35] D. Bommes, H. Zimmer, L. Kobbelt, Mixed-integer quadrangula- 1153
1079 tion, ACM Trans. Graph. 28 (3). doi:[10.1145/1531326.1531383](https://doi.org/10.1145/1531326.1531383). 1154
1080 URL <https://doi.org/10.1145/1531326.1531383> 1155
1081 [36] A. Jacobson, D. Panozzo, et al., libigl: A simple C++ geometry 1156
1082 processing library, <https://libigl.github.io/> (2018). 1157
1083 [37] R. Sauer, Differenzengeometrie, Springer, 1970. 1158
1084 [38] J. C. Maxwell, On reciprocal figures, frames, and diagrams of 1159
1085 forces, Trans. R. Soc. Edinburgh 26 (1872) 1–40. 1160
1086 [39] W. Blaschke, Vorlesungen über Differentialgeometrie, Vol. 2, 1161
1087 Springer, 1923. 1162
1088 [40] H. Pottmann, Y. Liu, Discrete surfaces in isotropic geometry, in: 1163
1089 R. Martin, M. Sabin, J. Winkler (Eds.), Mathematics of Surfaces 1164
1090 XII, Springer Berlin Heidelberg, Berlin, Heidelberg, 2007, pp. 341– 1165
1091 363. 1166
1092 [41] D. Pellis, Quad meshes as optimized architectural freeform struc- 1167
1093 tures, Ph.D. thesis, Wien (2019). 1168
1094 [42] C. Millar, T. Mitchell, A. Mazurek, A. Chhabra, A. Beghini, 1169
1095 A. McRobie, W. Baker, On funicular gridshells and Airy stress 1170
1096 functions, in: Proceedings of the IASS Symposium 2020/21, 2021. 1171
1097 URL [https://www.researchgate.net/publication/354118428_](https://www.researchgate.net/publication/354118428_1172)
- On_funicular_gridshells_and_Airy_stress_functions
- [43] C. Millar, T. Mitchell, A. Mazurek, A. Chhabra, A. Beghini, J. N. Clelland, A. McRobie, W. F. Baker, On designing plane-faced funicular gridshells, manuscript submitted for publication (2021).
- [44] X. Tellier, C. Douthe, L. Hauswirth, O. Baverel, Form-Finding with Isotropic Linear Weingarten Surfaces, in: Advances in Architectural Geometry, 2020, pp. 18–37.
URL https://www.researchgate.net/publication/361440116_Form-Finding_with_Isotropic_Linear_Weingarten
- [45] Y.-C. Chiang, Design and fabrication of shell structures: Aided by radial basis functions and reconfigurable mechanisms, Ph.D. thesis, Delft University of Technology (2022). doi:[10.7480/abe.2022.03](https://doi.org/10.7480/abe.2022.03).
- [46] T. Ivey, Surfaces with orthogonal families of circles, Proc. Amer. Math. Soc. 123 (1995) 865–872.
- [47] H. Sachs, Die Strahlflächen mit durchwegs ebenen Orthogonaltrajektorien der Erzeugenden, Arch. Math. 21 (1970) 437–444.
- [48] W. Wunderlich, Flächen mit ebenen Fallinien, Monatsh. Math. 65 (1961) 291–300.
- [49] W. Wunderlich, Flächen mit Kegelschnitten als Fallinien, J. Reine Angew. Math. 208 (1961) 204–220.
- [50] W. Wunderlich, Römerflächen mit ebenen Fallinien, Annali di Matematica pura ad applicata 57 (1962) 97–108.
- [51] W. Wunderlich, Betrag- und Potentialflächen mit ebenen Fallinien, Sitzungsber. Österr. Akad. Wiss., Math.-Naturw. Kl. 170 (1962) 105–120.
- [52] H. Trautwein, Neue Flächen mit ebenen Fallinien, Ph.D. thesis, TU Munich (1996).
- [53] C. Tang, X. Sun, A. Gomes, J. Wallner, H. Pottmann, Form-finding with polyhedral meshes made simple, ACM Trans. Graph. 33 (4) (2014) 70:1–70:9.
- [54] H. Pottmann, M. Hofer, Geometry of the squared distance function to curves and surfaces, in: H.-C. Hege, K. Polthier (Eds.), Visualization and Mathematics III, Springer, 2003, pp. 223–244.
URL <http://www.geometrie.tuwien.ac.at/ig/papers/pot121.pdf>
- [55] J. Wang, C. Jiang, P. Bompas, J. Wallner, H. Pottmann, Discrete line congruences for shading and lighting, Computer Graphics Forum 32 (5) (2013) 53–62. doi:<https://doi.org/10.1111/cgf.12172>.
URL <https://onlinelibrary.wiley.com/doi/abs/10.1111/cgf.12172>